UNITED STATES
DEPARTMENT OF
COMMERCE
PUBLICATION

NBS TECHNICAL NOTE 643

# Measurement of rf Power and Attenuation Using Superconducting Quantum Interference Devices

U.S.
DEPARTMENT
OF
COMMERCE
National
Bureau
of
Standards

## NATIONAL BUREAU OF STANDARDS

The National Bureau of Standards [1] was established by an act of Congress March 3, 1901. The Bureau's overall goal is to strengthen and advance the Nation's science and technology and facilitate their effective application for public benefit. To this end, the Bureau conducts research and provides: (1) a basis for the Nation's physical measurement system, (2) scientific and technological services for industry and government, (3) a technical basis for equity in trade, and (4) technical services to promote public safety. The Bureau consists of the Institute for Basic Standards, the Institute for Materials Research, the Institute for Applied Technology, the Institute for Computer Sciences and Technology, and the Office for Information Programs.

**THE INSTITUTE FOR BASIC STANDARDS** provides the central basis within the United States of a complete and consistent system of physical measurement; coordinates that system with measurement systems of other nations; and furnishes essential services leading to accurate and uniform physical measurements throughout the Nation's scientific community, industry, and commerce. The Institute consists of a Center for Radiation Research, an Office of Measurement Services and the following divisions:

Applied Mathematics — Electricity — Mechanics — Heat — Optical Physics — Nuclear Sciences [2] — Applied Radiation [2] — Quantum Electronics [3] — Electromagnetics [3] — Time and Frequency [3] — Laboratory Astrophysics [3] — Cryogenics [3].

**THE INSTITUTE FOR MATERIALS RESEARCH** conducts materials research leading to improved methods of measurement, standards, and data on the properties of well-characterized materials needed by industry, commerce, educational institutions, and Government; provides advisory and research services to other Government agencies; and develops, produces, and distributes standard reference materials. The Institute consists of the Office of Standard Reference Materials and the following divisions:

Analytical Chemistry — Polymers — Metallurgy — Inorganic Materials — Reactor Radiation — Physical Chemistry.

**THE INSTITUTE FOR APPLIED TECHNOLOGY** provides technical services to promote the use of available technology and to facilitate technological innovation in industry and Government; cooperates with public and private organizations leading to the development of technological standards (including mandatory safety standards), codes and methods of test; and provides technical advice and services to Government agencies upon request. The Institute consists of a Center for Building Technology and the following divisions and offices:

Engineering and Product Standards — Weights and Measures — Invention and Innovation — Product Evaluation Technology — Electronic Technology — Technical Analysis — Measurement Engineering — Structures, Materials, and Life Safety [4] — Building Environment [4] — Technical Evaluation and Application [4] — Fire Technology.

**THE INSTITUTE FOR COMPUTER SCIENCES AND TECHNOLOGY** conducts research and provides technical services designed to aid Government agencies in improving cost effectiveness in the conduct of their programs through the selection, acquisition, and effective utilization of automatic data processing equipment; and serves as the principal focus within the executive branch for the development of Federal standards for automatic data processing equipment, techniques, and computer languages. The Center consists of the following offices and divisions:

Information Processing Standards — Computer Information — Computer Services — Systems Development — Information Processing Technology.

**THE OFFICE FOR INFORMATION PROGRAMS** promotes optimum dissemination and accessibility of scientific information generated within NBS and other agencies of the Federal Government; promotes the development of the National Standard Reference Data System and a system of information analysis centers dealing with the broader aspects of the National Measurement System; provides appropriate services to ensure that the NBS staff has optimum accessibility to the scientific information of the world. The Office consists of the following organizational units:

Office of Standard Reference Data — Office of Technical Information and Publications — Library — Office of International Relations.

---

[1] Headquarters and Laboratories at Gaithersburg, Maryland, unless otherwise noted; mailing address Washington, D.C. 20234.
[2] Part of the Center for Radiation Research.
[3] Located at Boulder, Colorado 80302.
[4] Part of the Center for Building Technology.

# Measurement of rf Power and Attenuation Using Superconducting Quantum Interference Devices*

R. A. Kamper and M. B. Simmonds
Cryogenics Divison

C. A. Hoer and R. T. Adair
Electromagnetics Division

Institute for Basic Standards
National Bureau of Standards
Boulder, Colorado 80302

*This work was carried out at the National Bureau of Standards, and was partially supported by the DoD Calibration Coordination Group (CCG):

** Army Metrology Center, Huntsville, Alabama
Navy Metrology Center, Pomona, California
Air Force Metrology Center, Newark, Ohio

** 1973 Chairman, M.L. Fruechtenicht, AMSMI-M


U.S. DEPARTMENT OF COMMERCE, Frederick B. Dent, Secretary
NATIONAL BUREAU OF STANDARDS, Richard W. Roberts, Director

Issued August 1973

**National Bureau of Standards Technical Note 643**

Nat. Bur. Stand.(U.S.), Tech. Note 643, 93 pages (August 1973)
CODEN: NBTNAE

For sale by the Superintendent of Documents, U.S. Government Printing Office, Washington, D. C. 20402
(Order by SD Catalog No. C13.46:643). Price $1.00

CONTENTS

Figures

Figures continued



Tables

# Measurement of rf Power and Attenuation Using Superconducting Quantum Interference Devices*

R. A. Kamper, M. B. Simmonds†, C. A. Hoer, and R. T. Adair

This report is the product of the first two years' work on a project to exploit an entirely new principle for the measurement of rf power and attenuation, namely the Superconducting QUantum Interference Device (SQUID). This is a simple circuit of superconducting metal, operating at a very low temperature in a bath of liquid helium. It functions as a sensor of magnetic flux with an almost perfectly periodic response over a wide dynamic range. It may therefore be used to measure dc or rf electrical quantities such as current, power, attenuation, etc., in circuits inductively coupled to it. Measurements of these quantities can be made by counting off periods in the response of the SQUID (flux quanta) in the same way that we measure length with a laser by counting off wavelengths of light.

This work is partly funded by the CCG under project number 72-72. It has reached the stage of a demonstration that the new principle can indeed be used for precise measurement. We have developed and tested prototype systems for measuring power and attenuation as accurately as we can test by the conventional means available to us. A single calibration with dc is required to measure absolute rf power in the range of frequency from 0 to 1 GHz at levels from $10^{-8}$ W to $10^{-3}$ W with an uncertainty of ±0.1 dB at the port of the SQUID. Transferring this measurement to calibrate a source of power would require a proper evaluation of the intervening network over the full range of frequency. We have demonstrated the feasibility of extending our measurements of power to much lower levels. No external calibration is required to measure rf attenuation directly over a dynamic range of 45 dB with an rms deviation of ±0.002 dB from calibrations performed by the NBS Calibration Service.

---

*This work was carried out at the National Bureau of Standards, and was partially supported by the DoD-CCG.

†NRC-NBS Postdoctoral Research Associate, 1971-73.

After an elementary exposition of the basic principles of our technique, we describe: the SQUIDs themselves; the prototype systems we have developed to measure rf power and attenuation; systematic errors and fundamental limitations of the measurements that can be performed with them; and the obvious and immediate improvements that can be applied to them. We reserve an appendix for detailed drawings and instructions for the fabrication of components.

In order to make this report self-contained, we have included the material from previous reports that has successfully withstood the test of time.

Key Words: Josephson effect; quantum interference; rf attenuation; rf measurement; rf power; superconductivity.

## 1. TECHNICAL BACKGROUND: QUANTUM INTERFERENCE DEVICES

The devices which form the subject of this report are based on the properties of superconductors. These are a class of metals which make a thermodynamic transition into a state characterized by zero electrical resistance when cooled below a temperature of a few kelvin. This transition temperature is a property of the individual metal, but does not exceed 21 K for any known superconductor. Above this temperature superconductors have no common feature to distinguish them from other metals. Superconducting devices must therefore operate at a suitably low temperature, and in practice this is usually maintained by immersing them in liquid helium. This is no longer inconvenient as it once was. Liquid helium is readily available; compact, portable containers exist which can give an operating time exceeding 30 hours with each filling of one liter of liquid [1][1]. Closed cycle refrigeration is another possibility. It is presently under commercial development.

The particular aspect of superconductivity that concerns us here is the Josephson effect. This takes place at an electrical contact between superconductors. The contact must be weak enough to restrict the flow of current but stable enough for use in a practical device. The transfer of current across such a contact (known as a Josephson junction) is controlled by processes distributed through the entire superconducting circuit connected to it [2].

There are several practical ways of making Josephson junctions. An ideal junction might consist of two superconductors separated by a vacuum gap about 10Å ($10^{-7}$ cm) wide and perhaps a square millimeter in area. Electrons would cross this gap by the quantum mechanical tunnel effect [3]. The nearest practical approach consists of a strip of thin film of one superconductor deposited on an insulating substrate

[1] Figures in brackets indicate the literature references at the end of this paper.

such as glass, quartz, or sapphire. Its surface is covered with an insulating barrier of the desired thickness (usually by oxidation of the metal), and then a strip of thin film of the second superconductor is deposited across the first to complete the junction. The barrier does not need to be an insulator. A layer of normal metal such as copper, about $10^{-4}$ cm thick [4], or a semiconductor [5], will work instead. Another approach is to use a continuous strip of superconducting thin film with a very narrow constriction [6] (about one micrometer wide). The electrical characteristics of this microbridge structure differ from those of crossed film junctions, but the similarities are sufficient for many practical purposes. An intermediate approach is to press a slender point on one superconductor lightly against the other to form a point contact junction [7]. It is not quite clear whether a surface layer formed by atmospheric corrosion forms an insulating barrier, or if the narrow contact area functions as a microbridge. However, point contacts have the great advantage that they can be adjusted while in operation and they work very well. The more permanent structures such as crossed film junctions and microbridges have the compensating advantage of greater mechanical stability. Chapter 2 of this report will discuss junctions in greater detail.

Superconductors commonly used to make Josephson junctions are lead, tin, indium, niobium, tantalum, etc. It is not important whether the same or two different superconductors are used to form a junction.

In addition to the usual leakage and displacement currents which flow through any metallic contact, a Josephson junction passes a component of current (the "Josephson current") which is controlled by conditions in the superconductors on either side. If they are connected together to form a loop closed by the junction, then the Josephson current $I_s$ depends upon the magnetic flux $\varphi$ linking the loop:

$$I_s = I_c \sin(2\pi \varphi/\varphi_o). \quad (1)$$

$I_c$ depends only on the strength of the particular contact. The quantity $\varphi_o$ is a fundamental constant of nature known as the flux quantum

$$\varphi_o = h/2e \quad (2)$$

where $h$ is Planck's constant and $e$ is the charge on the electron. The numerical value of $\varphi_o$ is $2.0678538 \times 10^{-15}$ $Tm^2$.

This arrangement of a small superconducting loop closed by a Josephson junction is the basic form of the SQUID, an acronym for Superconducting QUantum Interference Device. Since this device is the heart of the whole project, we will analyze its properties a little further, following Silver and Zimmerman [8].

The magnetic flux $\varphi$ linking the loop (equation 1) is the sum of two terms

$$\varphi = \varphi_x + LI_s \quad (3)$$

where $\varphi_x$ is the flux from some external source driving the device and $L$ is the inductance of the loop. Strictly speaking, the current $I_s$ in equation (3) is the total current (including leakage, etc.) flowing through the junction. However, SQUIDs are usually designed so that the Josephson current (equation 1) is the dominant term, so we may obtain an approximate understanding of the action of the device by neglecting the other contributions to the current. We may therefore combine equations (1) and (3):

$$\varphi = \varphi_x + LI_c \sin(2\pi \varphi/\varphi_o) \quad (4)$$

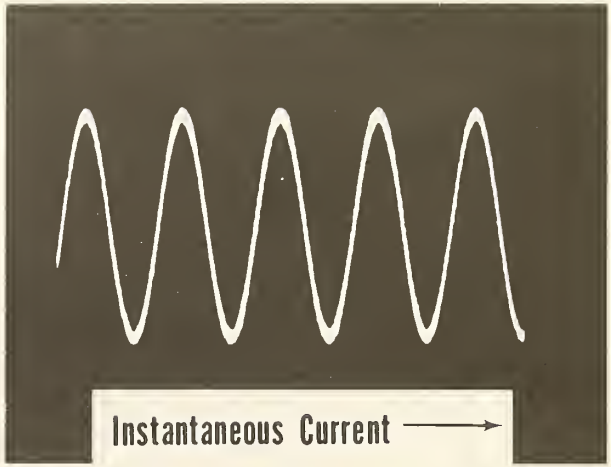


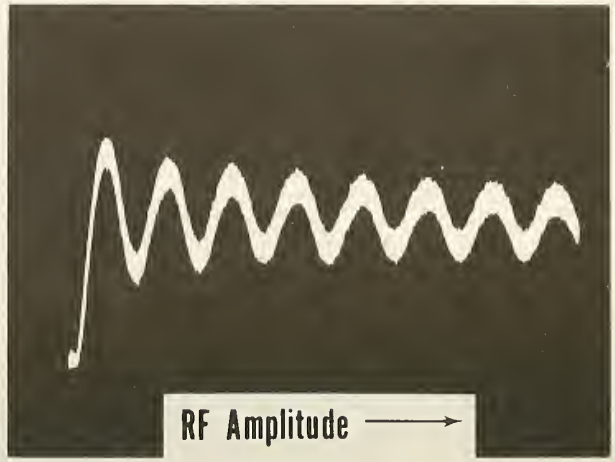


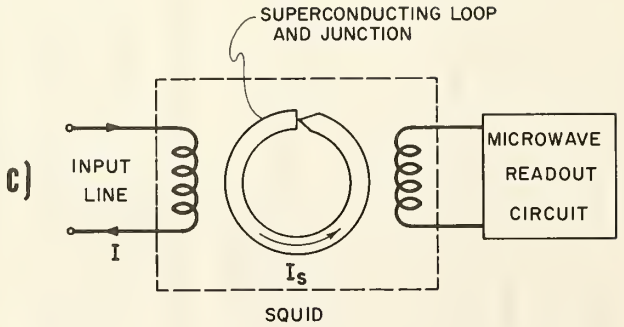


Figure 1 (a,b,c). The response of the microwave (power) reflection coefficient of the broadband SQUID to variations in current I in the input line.

a) the basic response to slow variations in current;
b) the averaged response to a slowly modulated rf current;
c) basic SQUID system, defining components and currents.

or alternatively $$I_s = I_c \sin\left[2\pi(\varphi_x + LI)/\varphi_o\right] . \quad (5)$$

Inspection of equation (5) shows that the current $I_s$ has a periodic dependence on the external magnetic flux $\varphi_x$. If we add any whole multiple of $\varphi_o$ to $\varphi_x$ the sine function is unchanged and therefore the current $I_s$ is unchanged also. Remembering that the emf $V$ around the loop is just $d\varphi/dt$, we can see that the device presents a nonlinear impedance to alternating current which is also a periodic function of the applied magnetic flux $\varphi_x$.

The standard technique for using a SQUID as a sensor of magnetic flux is to monitor this variation in impedance by coupling the device inductively to a readout circuit operating at some convenient radio frequency, as shown in figure 1 [8,9,10]. (These references give the details of readout circuits operating at 30 MHz, and the output signals that can be obtained.)

The SQUID derives its name from the fundamental process causing quantization of magnetic flux. Electrons behave like waves, with wavelength $\lambda$ proportional to the reciprocal of the momentum $p$

$$\lambda = h/p. \quad (6)$$

In a normal metal the electrons are scattered in such a short distance that they quickly lose coherence and so their wavelike nature is not obvious. In a superconductor, however, scattering is ineffective at disturbing the coherence of the waves, and interference may be observed in circuits with multiple paths. The momentum (and hence the wavelength) of the electrons in a superconducting circuit is controlled by magnetic flux, so the strange variation of current with magnetic flux in a SQUID (equation 5) comes about from interference between waves whose phase can be shifted magnetically.

Regardless of the origin of magnetic flux quantization, it has the potential to be a great boon to electrical metrology. In any circuit with stable geometry the magnetic flux $\varphi_x$ is proportional to the current I. The flux quantum is therefore a natural repeating unit with which to measure current just as the wavelength of light from a laser is used to measure length. SQUIDs absorb an infinitesimal amount of power from the source of magnetic flux, so the impedance of the circuit may be kept under control over a wide range of conditions. It is therefore easy to relate measured current to power and voltage.

The SQUID may be used to measure alternating current just as well as direct current. However, looking back at equation (5), it is evident that the only simple feature of the basic response of the SQUID to magnetic flux is its strict periodicity. This may be preserved provided that the frequency of the readout system is well above the frequency of the current to be measured. Another benefit of operating the SQUID at the highest possible frequency is the achievement of optimum sensitivity. The power available in the readout signal is theoretically proportional to its frequency up to some (as yet undetermined) limit. This is a common feature of parametric devices.

The first objective of the program was therefore to develop a broadband SQUID with a readout circuit operating at 9 GHz. This is suitable for measuring rf power at frequencies up to 1 GHz. We have developed several working versions of the SQUID, together with several microwave readout systems, operating at frequencies from 1 to 10 GHz, which we will describe in detail later in this report. A common feature of all of these is that the SQUID is inductively coupled to a coaxial line circuit (of 50 Ω characteristic impedance) in which power is to be measured.

The periodic response of the impedance of the SQUID to variations of magnetic flux driven by the current I in this circuit is monitored by a microwave system which detects variations in the microwave reflection coefficient of the SQUID.

The basic response of one of these systems, operating at 9 GHz, to the current to be measured is displayed in figure 1a. This is an oscilloscope display obtained with a slowly varying current. Monitored in this way, the periodic response of the SQUID to magnetic flux has degenerated into a simple and remarkably pure sine function (the second harmonic is 25 dB below the fundamental, and the third harmonic is 40 dB down). This is a feature of the broadband microwave readout system that is not necessarily shared by systems operating at lower frequencies.

Presented with an rf current, at the input line, the system records an average over a segment of figure 1a. The width of the segment is determined by the amplitude of the rf current, and its location can be moved by simultaneously applying a dc bias. As the amplitude of the rf current varies, this averaged response reflects the basic periodicity of the SQUID. This is shown in figure 1b, which is an oscilloscope display obtained by applying a slow amplitude modulation to an rf current at 65 MHz applied to the SQUID. A simple analysis shows, in the approximation that the basic response to current shown in figure 1a is a sine function $\sin(2\pi I/I_o)$, the averaged response to rf current shown in figure 1b is the zero order Bessel function $J_o(2\pi I/I_o)$. In both expressions $I_o$ is the current required to drive one quantum of magnetic flux into the SQUID. It may be determined with a single measurement using dc. Notice that the frequency does not enter explicitly into these expressions. We have developed a simple system to use a lock-in detector to locate the zeros of the Bessel function describing the response to rf current

shown in figure 1b. The values of the argument $2\pi I/I_o$ at these zeros have been computed and published in tables of Bessel functions [11]. They form the natural scale on which our new system of rf measurements is based. We have been able to locate the positions of the first 600 points on this scale, covering a dynamic range of 60 dB. We would probably be able to use many more with finer control on the rf level. We have made precise measurements of the locations of the first 100 points, covering a dynamic range of about 45 dB. We have shown that the scale is "true" to better than 0.002 dB rms in this range. Defining the performance of the new system more precisely than this will raise serious questions about the accuracy of the more conventional techniques we use for comparison.

The mode of operation we have just described essentially detects the "carrier" of the microwave signal reflected by the SQUID, at the same frequency as the incident wave. In response to magnetic flux from an rf current, the SQUID also generates sidebands displaced from the frequency of the incident wave by an amount equal to the frequency of the rf current. The same simple analysis we quoted before shows that the power in the nth sideband varies like the nth order Bessel function $J_n(2\pi I/I_o)$. In particular, the first sideband varies with amplitude of the rf current like the first order Bessel function $J_1(2\pi I/I_o)$. There are two benefits to be obtained from a system with a response of this form:

1) The first order Bessel function rises linearly from zero with small values of its argument. It therefore opens the possibility of making a linear detector for very weak signals, which can be calibrated by measuring the height and location of the first peak of the function. In contrast, the zero order function $J_o$ has a peak value at zero argument, and its slope is zero on this peak.

2) The zeros of $J_1$ are interleaved between those of $J_o$. Therefore a system displaying both these response functions simultaneously generates enough information to drive an up-down counter. This could follow arbitrary variations in rf current and automatically record the number of the nearest zero of $J_o(2\pi I/I_o)$. Obviously, this would be a major step towards a completely automatic system, especially if the high order zeros are used. The spacing between the 99th and 100th zeros is approximately 0.1 dB, and it diminishes (measured in dB) with increasing order number. Interpolation between zeros may not even be necessary for many purposes.

We have developed microwave systems capable of responding to the first sideband as well as the carrier. We will describe one of them in detail later in this report. It works, but it lacks the simple elegance of our system which responds to the carrier only.

In summary, we have demonstrated an entirely new system for making rf measurements. It can be made to constitute a negligible perturbation of the signal being measured, and therefore enables the impedance of a circuit to be kept under good control. Its response to rf current is of the form $J_n(2\pi I/I_o)$. The order $n$ is open for choice. Armed with a table of Bessel functions, this response can be translated into an accurate and practical scale for rf measurements.

So much for basic principles. The following sections will describe in greater detail what we have accomplished in various aspects of the implementation of these principles in practical systems for measuring rf power and attenuation.

## 2. MICROWAVE SQUIDS

Any SQUID must be designed to derive an optimum readout signal from the basic response to magnetic flux given by equations (4) and (5). This problem has been discussed extensively in the literature [8,9,12], and we have increased our own understanding with the aid of a special analog computer. It is not simple because of the highly non-linear processes involved. We can summarize the results in a set of notes on the choice of the various parameters:

Operating Level: The (microwave) readout system should be set to sweep the magnetic flux in the loop through one flux quantum $\varphi_o$ (peak to peak) during each cycle. Because of the periodicity of the response of the SQUID, good performance may also be obtained at simple multiples of this microwave flux level. However, this tends to cause trouble by saturating amplifiers without improving the signal.

Voltage: At the optimum operating level, the (microwave) voltage across the Josephson junction is of the order $\varphi_o f$, where $f$ is the microwave frequency.

Current: The amplitude of the microwave current flowing through the Josephson junction in the same condition is $I_c$ (equation 1). The maximum usable value of $I_c$ is controlled by the inductance of the loop. For the SQUIDs we have been working with, $I_c$ is of the order $10^{-6}$ A.

Inductance: We must satisfy the inequality $LI_c \leq \varphi_o$. Part of the reason for this may be seen by inspecting equation (5). If the current in the SQUID is to be sensitive to magnetic flux at the level of a single quantum, $\varphi_x (\approx \varphi_o)$ must at least be comparable to $LI$. Actually, the requirement is stronger than this. If $LI_c$ significantly exceeds $\varphi_o$, the simple periodic response of the SQUID to magnetic flux breaks down, to be replaced by an unstable behavior with multiple periodicity.

A reasonable inductance to aim for in a structure that is large enough to be coupled to a microwave circuit is about $2 \times 10^{-9}$ H, which gives an optimum value of $10^{-6}$ A for $I_c$.

Readout Signal Power: Putting together the quantities we have determined so far, we find that the maximum amount of power that the SQUID is able to put into modulation of the reflected microwave signal is about $2 \times 10^{-11}$ W at X-band. We arrange for the incident wave to be at a comparable level.

Coupling: Much of the previous discussion of coupling the SQUID to the readout circuit is specialized to a resonant circuit. However, the general conclusion is that critical coupling is optimum. The power absorbed by the SQUID should be equal to the power absorbed by the receiver. This is a criterion that can be used in a broadband system.

Using these principles as a guide, we have developed two new basic forms of the SQUID:

1) a broadband SQUID with a readout system operating at X-band (9 GHz). This is intended for measuring rf power in the range of frequency from 0 to 1 GHz. We have used it with several variations of the circuit for coupling to the rf power to be measured, making different "trade-offs" between sensitivity and bandwidth.

2) a resonant SQUID, tuned to a readout system operating at L-band (1.2 GHz). This is intended for measuring attenuation at 30 MHz. It would function equally well at any frequency from 0 to 100 MHz.

We will describe these two types of SQUID in greater detail in the following two sections of this chapter. The appendix to this report contains workshop drawings and notes on the fabrication of these devices.

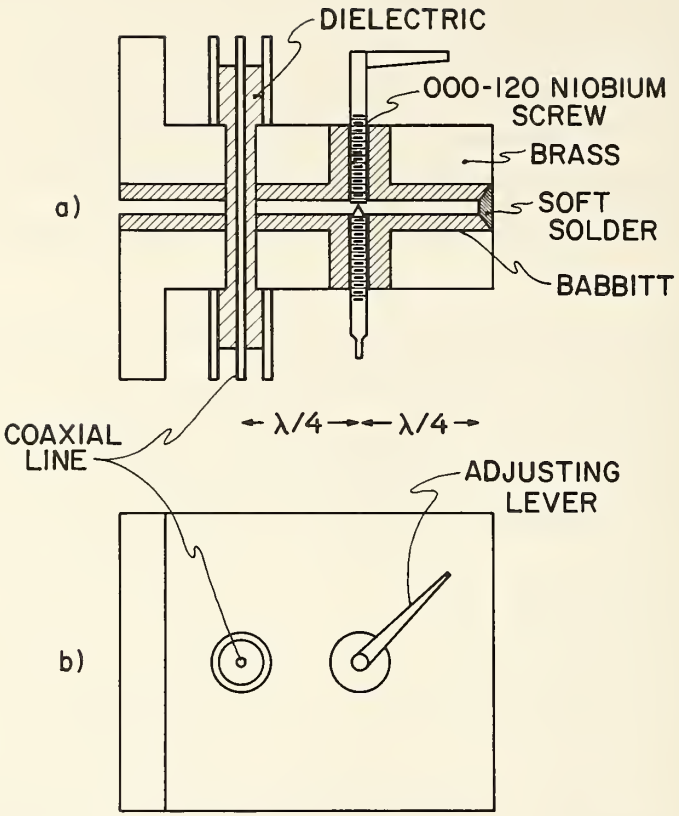


Figure 2. The broadband microwave SQUID. Some dimensions have been exaggerated for clarity. The internal dimensions are: 3.0 cm long, 2.3 cm wide, 0.025 cm high. It is connected to the microwave readout system via a linear taper section of waveguide 10 cm long, to transform its impedance up to WR90 waveguide.

The heart of any SQUID is the Josephson junction. For early tests of new forms of the SQUID we have used simple point contacts between small niobium screws, one sharpened and the other flat-tipped. In a final section of this chapter we will describe some more sophisticated junctions we have developed for use in more permanent instruments.

## 2.1 The X-band SQUID

The basic form of this SQUID is sketched in figure 2. It consists of a short section of rectangular X-band waveguide, reduced in the E-direction to a height of 0.25 mm in order to give a characteristic impedance of 10 Ω (at the midpoint). It is lined with superconducting metal (babbitt). The Josephson junction closing the loop is placed on the center line a quarter wavelength from the short circuit termination which forms the loop itself.

The current to be measured is coupled inductively to the active part of the SQUID. In the version shown in figure 2 this is accomplished by passing the center conductor of the coaxial input line through the device parallel to the E-field. This mode of coupling has the merits of a very broad bandwidth (the lowest resonance is at the cutoff frequency of the waveguide, approximately 6.6 GHz), and a very small perturbation of the input line. It is equivalent to a series inductance of about $10^{-10}$ H. Even without capacitive compensation this causes a smaller reflection than most rf connectors. The sensitivity of this version of the SQUID to current in the input line is only moderate. Depending upon the position of the input line relative to the Josephson junction, the current $I_o$ required to couple one flux quantum into various SQUIDs we have tested varies from 16 μA (line 2 mm from point) to 100 μA (line 1 cm from point, towards the side of the waveguide). The sensitivity could be reduced arbitrarily by moving the input line further away.

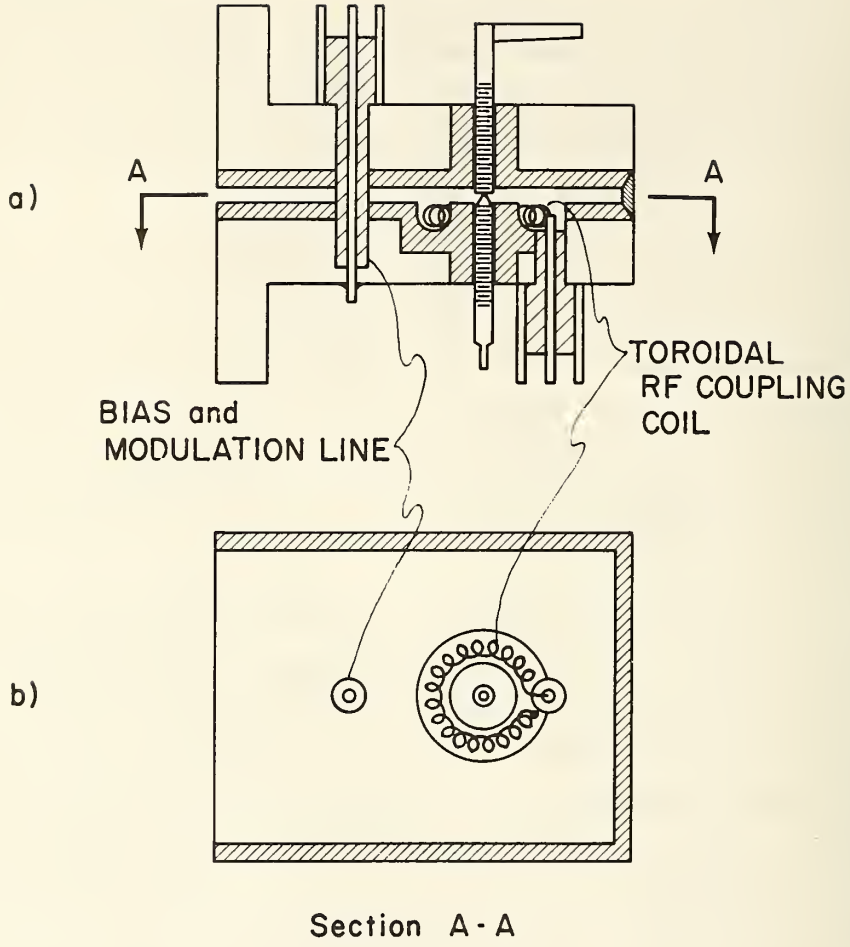


Figure 3. Modified version of the broadband microwave SQUID (figure 2). The sensitivity to rf current has been increased by the addition of a toroidal input coupling coil. A separate input line is provided for bias and modulation.

We often provide our SQUIDs with a pair of input lines. One of them is carefully terminated by a matched load and carries the rf current to be measured. The other is usually terminated by a simple short and carries dc bias and modulation at an audio frequency (usually 1 kHz). Although the input lines are drawn on the center line of the SQUID for clarity in figures 2 and 3, we usually place them toward the sides. Because of the high impedance of the 50 Ω coaxial lines compared with the 10 Ω waveguide, the loading of the microwave system is small.

In order to increase the sensitivity of the SQUID to current in the input line, we adopted the toroidal coupling coil shown in figure 3. This acts as a transformer with a multi-turn primary and a single-turn secondary. With a 50-turn coil we have observed $I_o$ to be down to 1 μA, or 24 dB less than the minimum we have observed with the broadband arrangement of figure 2. The price one pays is reduction of the bandwidth. This same 50-turn coil has an inductance of $1.5 \times 10^{-7}$ H and a self-resonant frequency of 200 MHz. For maximum sensitivity, we connect one end of the coupling coil to ground and use a tuned matching network. The objective is to dissipate as much as possible of the rf power to be measured in the Josephson junction rather than a passive load outside the SQUID. We will discuss our experience with impedance-matching networks in chapter 3 of this report.

Figure 4 is a photograph of one of our X-band SQUIDs. The tapered waveguide section (10 cm long) connects it to the WR90 waveguide of the microwave readout system. This particular SQUID has a toroidal coupling coil for the rf signal, and a weakly coupled input for bias and modulation, attached respectively to the two coaxial line connectors. This picture also shows the mechanism for adjusting the point contact Josephson junction. One of the niobium screws is spot-welded to a small lever, which is actuated by a hook at the end of a push-rod.

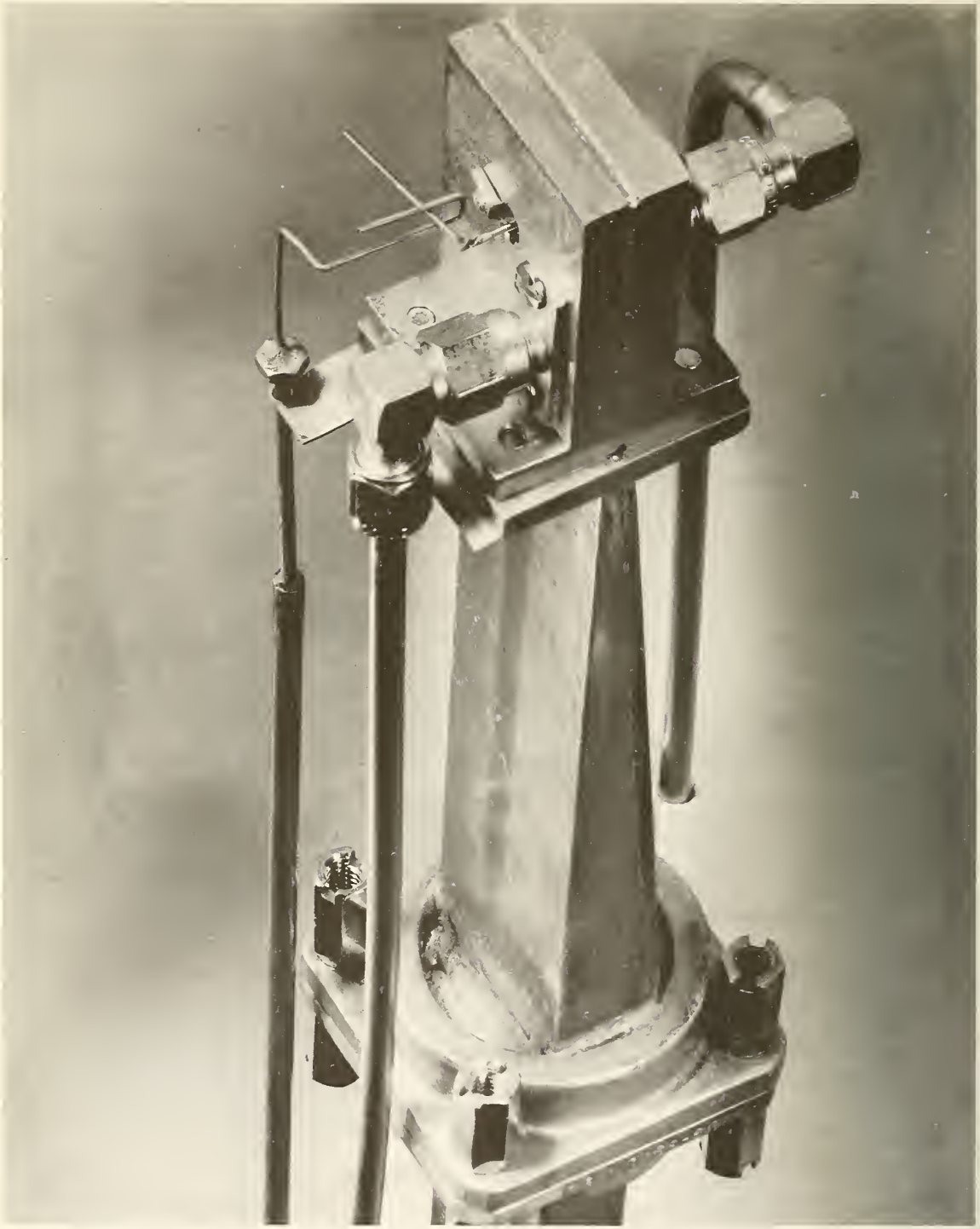

Figure 4. The broadband microwave (X-band) SQUID. The mechanism for adjusting the point contact via a push rod can be clearly seen.

This push-rod passes out of the cryostat to a micrometer drive. When the point is adjusted, the hook is backed off a short distance to prevent the push-rod from transmitting mechanical shocks. A small spring holds the niobium screw in place.

The microwave readout system we use with all these SQUIDs is shown schematically in figure 5. The drive power is generated by a klystron oscillator and passes to the SQUID through several attenuators and a directional coupler (about 90 dB total attenuation). The signal reflected from the SQUID is amplified by a chain of tunnel diode amplifiers (40 dB gain, 1 GHz bandwidth) and detected with a crystal rectifier. This is the system that was used to obtain the displays shown in figure 1. The microwave power level at the SQUID was $7 \times 10^{-11}$ W, and the reflected signal varied by 4 dB between the peaks and valleys of the quantum interference pattern. The amplitude of the corresponding signal at the crystal detector was a few mV.

## 2.2 The L-band SQUID

For purposes which do not require the full bandwidth of the X-band SQUID, one should consider the merits of a device operating at a lower frequency. In particular, L-band amplifiers cost an order of magnitude less than X-band amplifiers of comparable noise figure, and these are the most expensive repeated components of systems using multiple SQUIDs. We developed our L-band SQUID for a system using two SQUIDs to measure attenuation at 30 MHz, which we will describe in chapter 4 of this report.

Figures 6 and 7 show a sketch and a photograph, respectively, of the L-band SQUID. It is a re-entrant cavity that resonates at 1.2 GHz with a loaded Q of about 25. The coffin-like shape was chosen to facilitate packing multiple SQUIDs into a confined space in a small

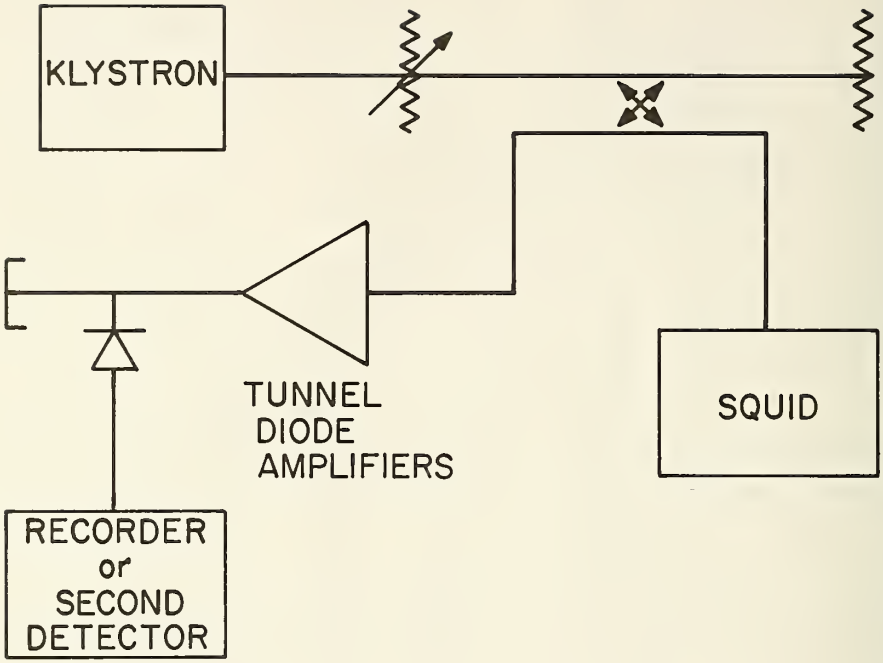


Figure 5. The basic crystal-video microwave readout system used to obtain the responses shown in figure 1.

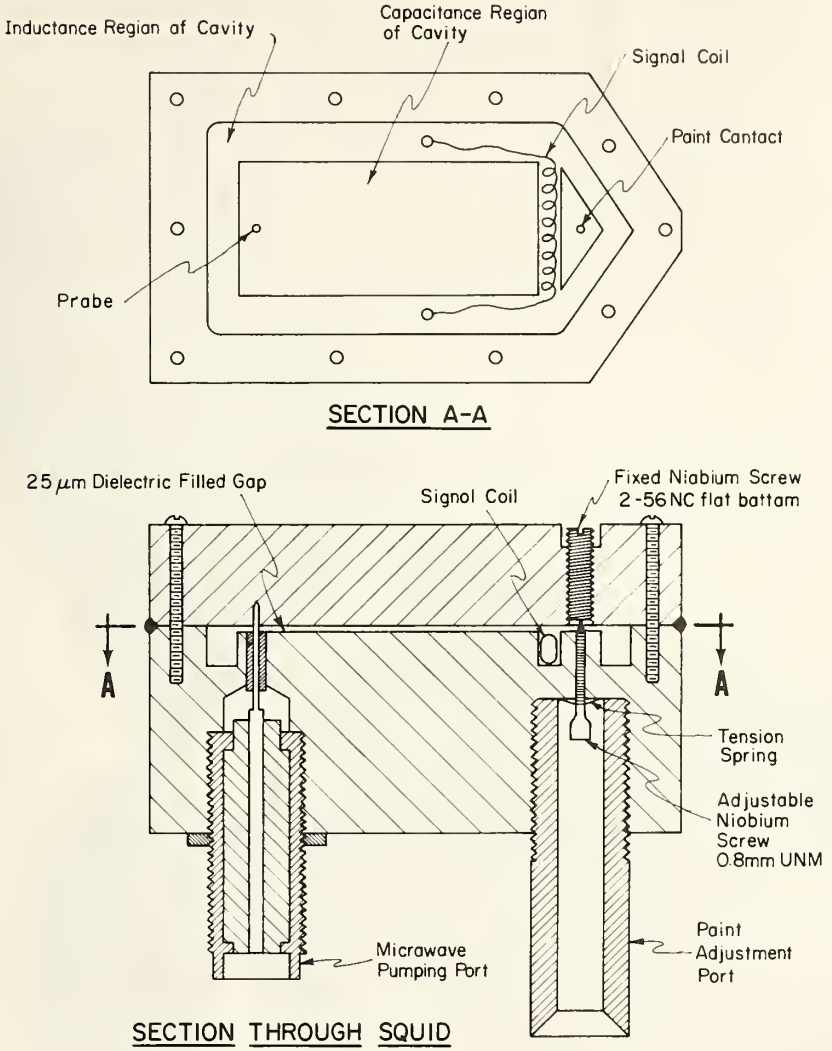


Figure 6. Resonant L-band SQUID. This is a re-entrant cavity with the point contact and the microwave coupling placed at points chosen to match impedances.

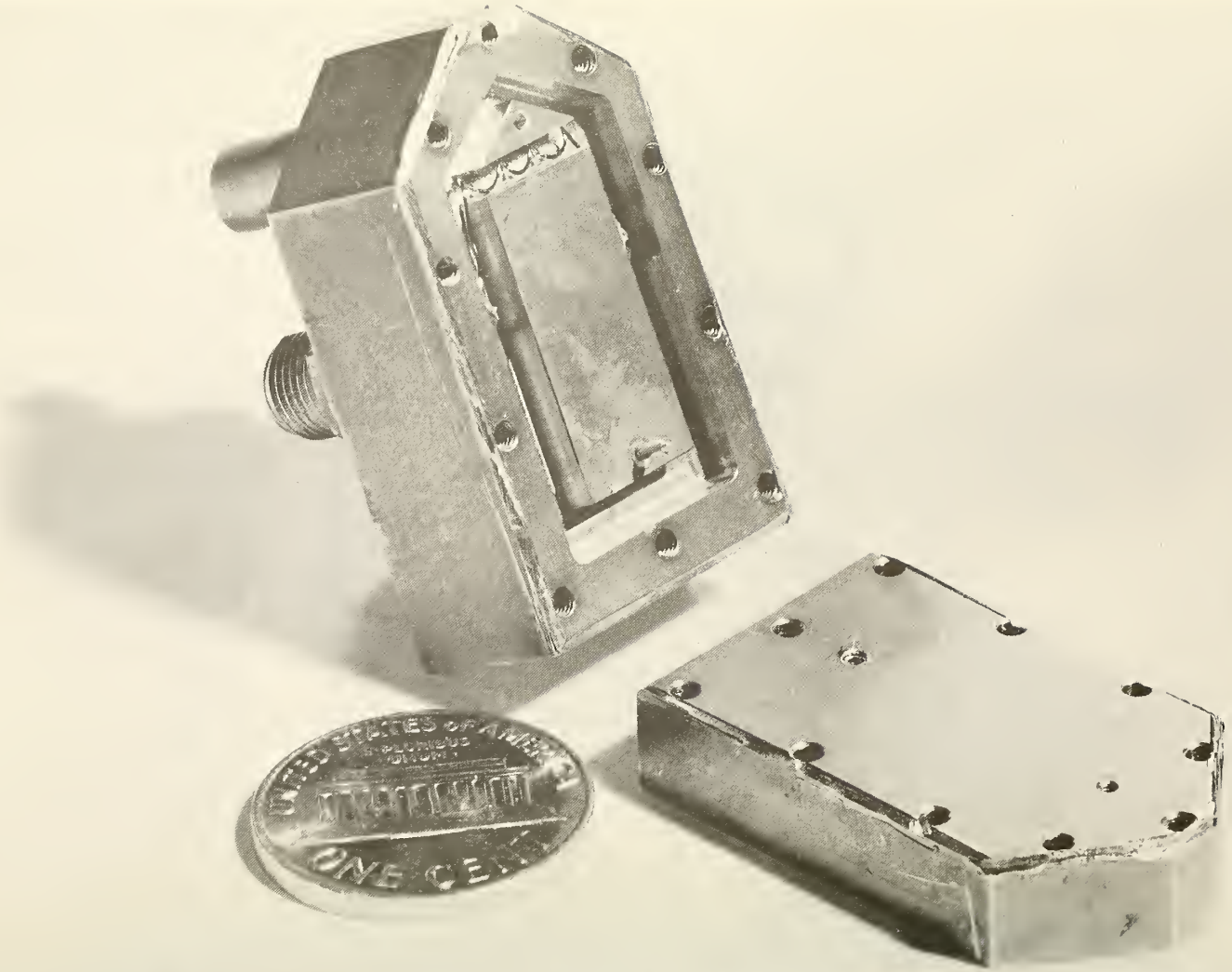


Figure 7. Resonant L-band SQUID, showing the rf input coupling coil and the connection for the microwave drive.

cryostat. The microwave readout system is the same in principle as the one shown in figure 5, with the substitution of L-band components connected via 50 Ω coaxial line. It is critically coupled to the cavity of the SQUID. The signal at 30 MHz to be measured is coupled in via a 3-turn coil terminated by a 50 Ω load connected directly to the SQUID. It requires 10 μA to induce a magnetic flux of one quantum. We chose this value of $I_o$ for a convenient power level for measuring attenuation; it can be adjusted over a range of about 20 dB by changing the number of turns on the coil.

Both this SQUID and the X-band SQUIDs we described in the previous section generate readout signals close to the theoretical optimum power.

## 2.3 Josephson Junctions

As a part of our effort to make these microwave SQUIDs more straightforward to use for routine calibration services, we have tried various alternatives to the simple point contact mentioned at the beginning of this chapter. Two of these will be described in detail, both because they have certain advantages over the simple point contact, and because they are illustrative of the basic problems and considerations encountered in designing Josephson junctions for quantum interference devices.

Thin Film Junctions: The most obvious advantage of using an evaporated film junction is its complete insensitivity to mechanical and thermal shock.

As we have already mentioned, junctions may be formed by evaporating one superconducting film over the top of a second, oxide-covered, superconducting film. Indeed, this is the classical form of the Josephson junction for observations of supercurrent tunneling.

However, this classical form of oxide barrier tunneling junction has never been successfully used in rf-biased SQUIDs, the reason being that the large capacitance and small conductance of such junctions causes switching and hysteresis in their characteristic current-voltage curves [13]. When they are placed in a low inductance loop (as in a SQUID) they ring incoherently, precluding the observation of quantum interference. A less obvious problem with these junctions is that their relatively large area (typically 0.1 $mm^2$) allows their critical current to be suppressed by magnetic fields of less than $10^{-4}$ T. This is inconvenient for a device which must be operated in the ambient field of the earth. Finally, the small thickness (typically 1.5 nm) of the oxide barrier in such structures makes them very susceptible to aging by thermal diffusion unless special precautions are taken during fabrication [14,15].

The use of a semiconducting material for the barrier in Josephson junctions is not new [5,16,17]; however, its suitability for use in SQUIDs has not been previously explored. Junctions of this type have several inherent advantages over oxide junctions for use in SQUIDs. The thicker barrier results in a much lower junction capacity, and reduces the problem of diffusion of the metals. The relatively large shunt conductance of semiconductor junctions helps damp the ringing which would plague ideal oxide junctions.

The large area of typical thin film junctions is an entirely separate problem. As we shall show, however, it is possible to reliably fabricate tunnel junctions with areas less than $2 \times 10^{-7}$ $cm^2$ by proper masking techniques.

We make these junctions by vapor depositing in an oil diffusion pumped high vacuum system. Typical operating pressures are about $5 \times 10^{-6}$ torr. Charges of the required material can be loaded remotely and evaporated to completion without breaking vacuum.

The geometry of the junctions is shown in figure 8. They consist of overlapping fingers of lead, separated by a finger of tellurium. This pattern is formed by using a contact mask which can be accurately moved between evaporations. A micrometer and a system of 10:1 mechanical reduction is used inside the vacuum system to accomplish this. A flexible shaft between the micrometer head and a vacuum feedthrough allows adjustment under vacuum. The micrometer setting can be read with a precision of about 5 μm through the glass bell jar, giving a reproducibility of better than 1 μm in the mask position. The total range of mask movement is about 0.5 mm.

The mask itself has two pointed openings. The points face each other, and are separated by 25 μm. The radius of curvature of the points is about 2 μm. These masks are made by forming the desired photo-resist image on a thin aluminum plate. A 3 μm coating of silver is then electrodeposited on the face of this plate, except for where the photo-resist pattern masks it. The aluminum backing is then removed with NaOH in the areas behind that pattern. The silver film provides a thin enough mask to have high definition, while the aluminum provides a rigid supporting structure.

The recipe for making the junctions is based on the technique first used by Giaver to handle the problem of shorting caused by pinholes [5]. A charge of lead is evaporated through the mask, which is in intimate contact with the quartz substrate. The mask is then moved in one direction by about 10 μm and 100 nm of tellurium is evaporated. The vacuum system is brought up to atmospheric pressure with dry oxygen and the substrate is heated to 60°C for about 2 hours. This process apparently oxidizes any lead which is showing through pinholes in the tellurium. The system is then re-evacuated and the substrate cooled to 20°C. The mask is translated 40 μm in the opposite direction and a

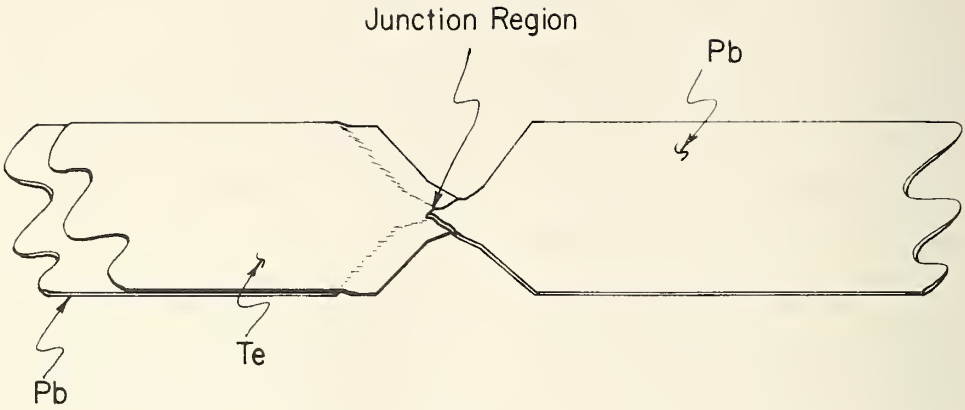


Figure 8. Tellurium-barrier tunnel junction. Successively evaporated films are displaced by small lateral movements of the mask.

final charge of lead is evaporated. For a 25 μm spacing of the fingers on the mask, this procedure gives a junction area of about $1.5 \times 10^{-7}$ $cm^2$ If the oxidation step is omitted the junctions are invariably shorted.

After fabrication the junctions are spin coated with a polyimide film. This film is baked on at 60°C for 15 minutes. This bake may result in additional annealing or diffusion within the junctions since it increased the critical current by a factor of two or more in some samples we tested before and after.

Junction characteristics appear to depend on many of the fabrication conditions. Temperature and time of the oxidation step, as well as tellurium thickness and substrate temperature during deposition all appear to be important.

The temperature dependence of critical current is qualitatively the same as that observed by Seto and Van Duzer [16]. Variations in supercurrent due to rotating our junctions in the earth's field are typically 15%. This is not a serious inconvenience.

These junctions show no reaction to thermal cycling; however, aging effects become apparent after several weeks. The rate of diffusion of lead into tellurium is high enough at room temperature that these junctions have an expected life of only a few months. Perhaps a doping technique such as that suggested by Cardinne, et al. [17, 18], could be used to form a more stable device.

We can use these junctions in a SQUID based on the design shown in figure 2. It is very difficult to make reliable contacts with low inductance between thin films and bulk materials. We avoid this problem by evaporating a lead film on the same substrate as the junction, in a C-shaped configuration placed so as to complete the superconducting loop. This is then inductively coupled to the main body of the SQUID, which is made from a solid block of

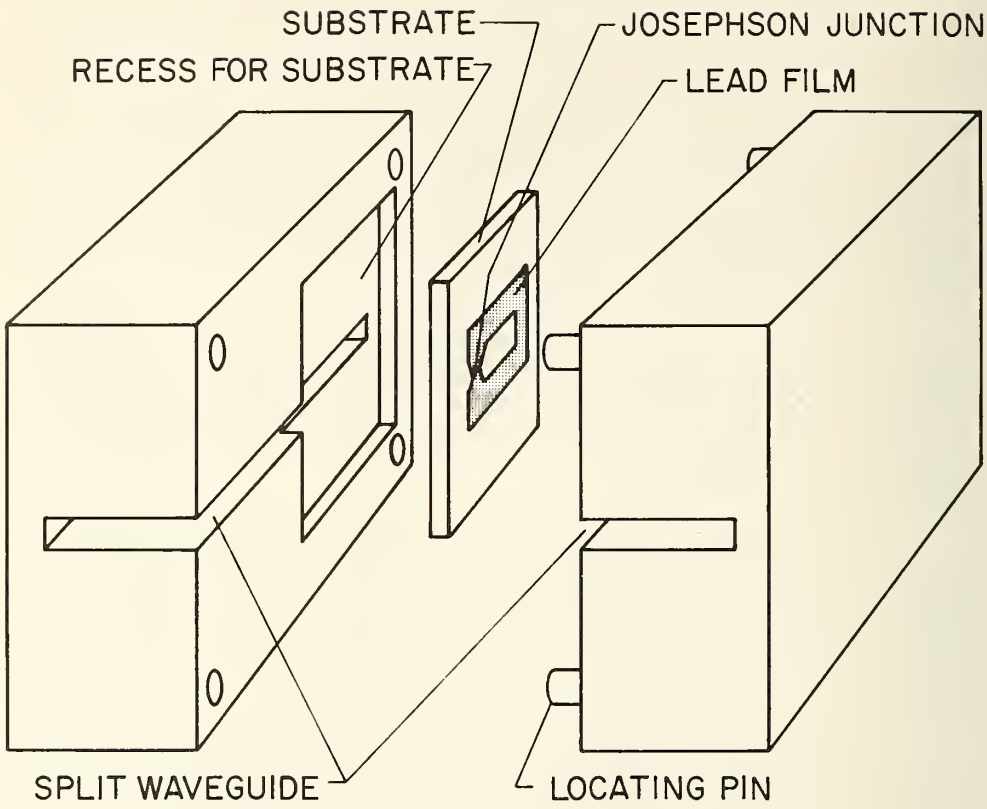


Figure 9. X-band SQUID using a tellurium-barrier tunnel junction inductively coupled to the waveguide structure. This is functionally equivalent to the SQUID shown in figure 2.

babbitt. The arrangement is shown in an exploded view in figure 9. The block is split in a plane containing the E direction and the center line of the waveguide section. A shallow recess in one face of the split accommodates the substrate carrying the thin film structure. When the device is assembled, it is connected to the microwave readout system (figure 5) via a tapered section of waveguide. Its performance is adequate, but the signal to noise ratio is about 5 dB lower than that of the equivalent SQUID with a point contact junction. Some attention to reducing stray inductance would probably improve its performance in this respect.

Improved Point Contacts: The usual configuration for a point contact junction is a small, sharp niobium screw touching a niobium anvil. The specific mechanism by which electron pairs cross this junction is not well understood. Tunneling through the native oxide or conduction through metallic filaments are two possibilities. In any event, the critical current is not a well-behaved function of contact pressure or apparent area. Since one is pushing two oxide covered surfaces together, adjustment can be a rather chanceful process, and must usually be repeated each time the junction is cooled. Zimmerman, et al. [9], have built point contact devices which survived cycling without adjustment, but for these the supporting structure had to be made entirely of niobium and of very rigid construction. They were also susceptible to shorting caused by even extremely small static electric discharges [19].

Our new technique for making point contact junctions appears to avoid most of these difficulties. A leaf spring of niobium is used in place of the rigid anvil; this is shown in figure 10. The surface of this spring, as well as the sharpened screw point, is buffed to an optical polish using rouge (the niobium must first be annealed, or extreme pitting will occur). The screws and springs are then placed in a nitrogen

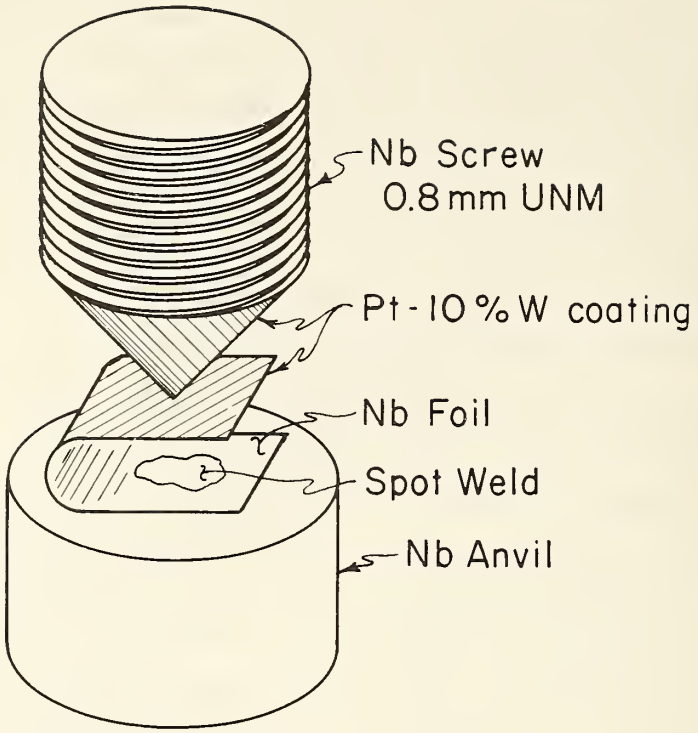


Figure 10. Stabilized point contact. This is a spring-loaded contact between niobium parts plated with a Pt-W alloy.

cooled sputtering can [20] in the vacuum system. After sputter cleaning these pieces for several minutes, a shutter is opened and the niobium is exposed to the ejecta from a Pt-W sputtering cathode. This cathode is a composite of platinum and tungsten sheet. Twenty percent of the exposed area of the cathode is tungsten, however the deposited alloy is only about 10 percent tungsten due to the higher sputter yield of platinum. The niobium pieces are coated with approximately 25 nm of this alloy.

The reasoning behind this design is that the Pt-10%W will form a durable, oxide free contact between the superconductors. The coatings are also thin enough that a suitable critical current can be sustained between contacting surfaces. The tungsten serves to raise the resistivity of the coating to approximately 80 $\mu\Omega$ cm. This minimizes the shunt conductance of the junction. Since there is no oxide to break through, the critical current is proportional to the contact area. A spring contact is used since it keeps a rather constant force on the contact in the face of thermal expansions and shocks. The contact is set by loading the spring with the niobium screw so that the microscopically sharp point is deformed into a 2 $\mu$m diameter disc. A 0.1 cm x 0.3 cm x 0.002 cm niobium spring, when displaced about 0.002 cm, gives the desired contact area.

The technique for adjusting these contacts is straightforward. The screw is advanced until electrical contact is made. This may be measured directly in a four-terminal arrangement, or inductively if the junction is in a SQUID. The 50-thread-per-centimeter screw is then given an additional 1/8 to 1/4 turn to load the spring and "form" the junction. If the sputtered coating is of the proper thickness, a suitable critical current will be observed upon cooling. Although the critical current tends to vary slightly each time such a device is cooled, there appears to be no trend toward deterioration.

These junctions can survive electrostatic discharges 100 times greater than that which would burn out an uncoated point contact of the same configuration. They behave electrically like an uncoated point contact with a shunt resistance of about 0.1 Ω. This does not noticeably degrade the readout signal obtainable from SQUIDs at frequencies ranging from 30 MHz to 9 GHz. It brings the bonus of a tendency to increase the purity of the sine-functional form of the basic response shown in figure 1, thereby improving the convenience and accuracy of rf measurements with these devices.

## 3. MEASUREMENT OF RF POWER

Our experience has shown that the measurement of rf power incident on the port of the SQUID at levels above $10^{-9}$ W is fairly straightforward. A properly terminated broadband SQUID requires but a single calibration with dc to cover a dynamic range of about 50 dB at any frequency up to 1 GHz. If power is to be measured at some arbitrary point in a circuit, then a careful evaluation of the reflections and attenuation in the network connecting that point to the SQUID is required at each frequency for which a measurement is to be made. This problem is common to all methods of measuring power, and limits the accuracy which can be attained.

Measurement of power at lower levels requires a system of greater complexity. A SQUID would be used to prepare a reference signal of known (and measurably high) power and approximately the same frequency as the signal to be measured. This would then be attenuated by a measured amount and compared with the unknown signal using a second SQUID for an indicator. SQUIDs can be used to calibrate the attenuators used at the frequencies at which measurements are to be made. We have tested various components of this system over a limited range of frequency to demonstrate its feasibility, but it is still at an early stage of development.

### 3.1 Power Levels Over One Nanowatt

We have already described, in chapter 2, the broadband SQUID and the basic form of its microwave readout system (see pages 19 and 20, figure 5). When an rf current $I \cos \omega t$ is passed through the appropriate port of the SQUID, the voltage $\overline{V}$ appearing at the microwave crystal detector has the approximate form

$$\overline{V} = V_o + V_1 J_o(2\pi I/I_o). \tag{7}$$

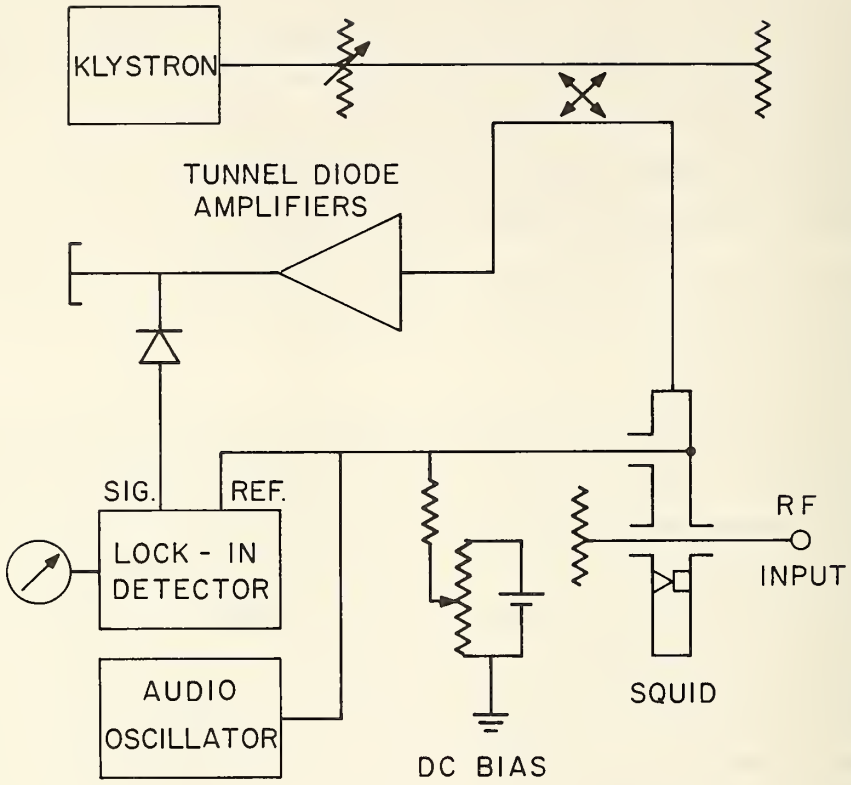


Figure 11. Basic system for measuring high (over $10^{-9}$ W) rf power. The lock-in detector is used to locate the nulls of the response function $J_o(2\pi I/I_o)$, where I is the amplitude of the rf current at the input.

In order to use this response for accurate measurements of $I$ we must locate the zeros of $J_o(2\pi I/I_o)$ accurately. This can be accomplished by adding low frequency modulation and a lock-in detection system, as shown in figure 11. The principle can be understood by contemplation of figure 1. The rf current generating the response shown in figure 1b is centered on one of the valleys of the basic response to current shown in figure 1a. If the dc bias point is changed by half of a flux quantum, the rf current will then be centered on a peak, and the response to rf current shown in figure 1b will be inverted. If the bias point is shifted back and forth in this manner at some audio frequency (say 1 kHz) then a lock-in detector can be used to pick off the component of the reflected wave that is modulated at this frequency. This passes through nulls at values of the rf amplitude $I$ corresponding to the zeros of $J_o(2\pi I/I_o)$. We will present a more formal analysis of the effects of modulation, dc bias level, distortion, etc., in chapter 5 of this report.

If the coaxial rf input line passing through the SQUID is properly terminated with a reflectionless 50 Ω load, then a single measurement of the quantity $I_o$ (equation 7), which can be performed with dc, is all that is required to measure rf power. We will show in chapter 4 that the response of the system is described by equation (7) with two orders of magnitude greater accuracy than is required to measure power to ± 0.1 dB.

In order to measure $I_o$ we apply a direct current to the rf input port of the SQUID. The basic response of the system then has the functional form

$$V = V_o + V_1 \sin(2\pi I/I_o) \tag{8}$$

where $I_o$ is the same quantity that appears in equation (7). The lock-in detection system can be used to locate the zeros of the sine function, and

a simple ammeter can be used to measure the change in current corresponding to the interval between them.

Since the SQUID is a magnetic sensor, it is necessary to take precautions to ensure that the direct current used for calibration follows the same path near the SQUID as the rf current on which measurements are to be made. In particular, one must avoid multiple return paths ("ground loops") between the coaxial lines. Because of inductive effects, rf current mainly flows inside the coaxial lines. It is not significantly perturbed by connections made outside the outer conductors. Direct current, however, simply follows the path of least resistance. We discovered the importance of this precaution because the first version of our system had the outer conductors of all the coaxial lines leading to the SQUID grounded to the top plate of the cryostat. The result was a discrepancy of 5% between the effective values of $I_o$ at low frequencies (below 1 kHz) and at high frequencies (above 100 kHz). This discrepancy was removed entirely by insulating the outer conductors of the coaxial lines from the top plate.

The other source of perturbation of the frequency response of the system is the assembly of lines, connectors, and components linking the SQUID with the point in a circuit where power is to be measured. Both attenuation and reflections can introduce frequency-dependent errors.

The most significant part of the attenuation occurs in the lines connecting the SQUID with the outside world. Copper conductors would introduce an unacceptably large heat leak ($\sim$ 10 W) into the cryostat, so instead we use semi-rigid coaxial line with stainless steel conductors and polyethylene dielectric. The inner conductor is plated with silver on copper to reduce the attenuation somewhat, but these lines are nearly one meter long and attenuate by 0.6 dB at 1 GHz. The attenuation depends upon both temperature and frequency. In order to make meaningful

measurements we stabilized the distribution of temperature by encasing these lines in copper pipes between the SQUID and a point well above the surface of the liquid helium. The high thermal conductance of the copper constrained the major part of the gradient of temperature to remain in the upper part of the cryostat, above the copper pipes, regardless of changes in the level of the liquid helium. We used two identical lines to take the rf signal from the top of the cryostat down to the SQUID and back up to a matched load. We measured the attenuation of the pair of lines in series, as a function of frequency, with an automatic network analyzer. We then assumed that the measured attenuation was equally divided between the two limbs. The result is shown in figure 12, which is a plot of attenuation, between the top of the cryostat and the SQUID, versus frequency. The measured attenuation is approximately proportional to the square root of the frequency, as one would expect from the rf skin effect.

Our procedure with reflections was to detect the worst offenders with a time domain reflectometer. After eliminating them we then measured the small residual reflections, at intervals of 10 MHz in the range of frequency from 100 MHz to 1 GHz, with the automatic network analyzer. The final version of the system had the rf lines soldered directly into the SQUID (no connectors); no sharp bends in the lines; and about 5 meters of the lossy line between the SQUID and the termination in order to attenuate (by several dB) the reflection from its connector. The residual reflections required corrections of less than $\pm$ 0.1 dB.

In order to test this system we set up the arrangement shown schematically in figure 13 and in a photograph in figure 14. We supplied rf power from a swept-frequency oscillator to a hybrid junction, which divided the power in constant ratio between the line to the SQUID and a bolometer power meter. The swept-frequency oscillator had a facility for amplitude

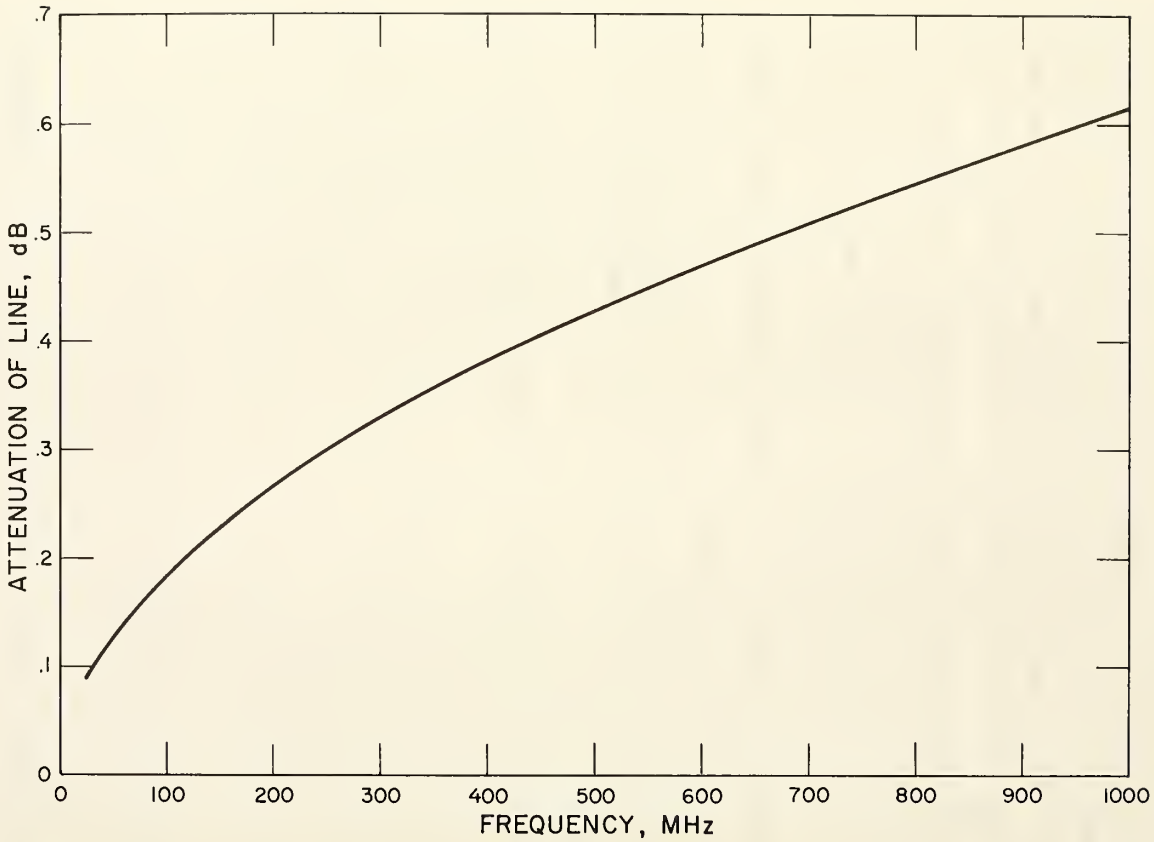


Figure 12. Variation with frequency of the attenuation of the stainless steel coaxial line connecting the SQUID to the top of the cryostat.

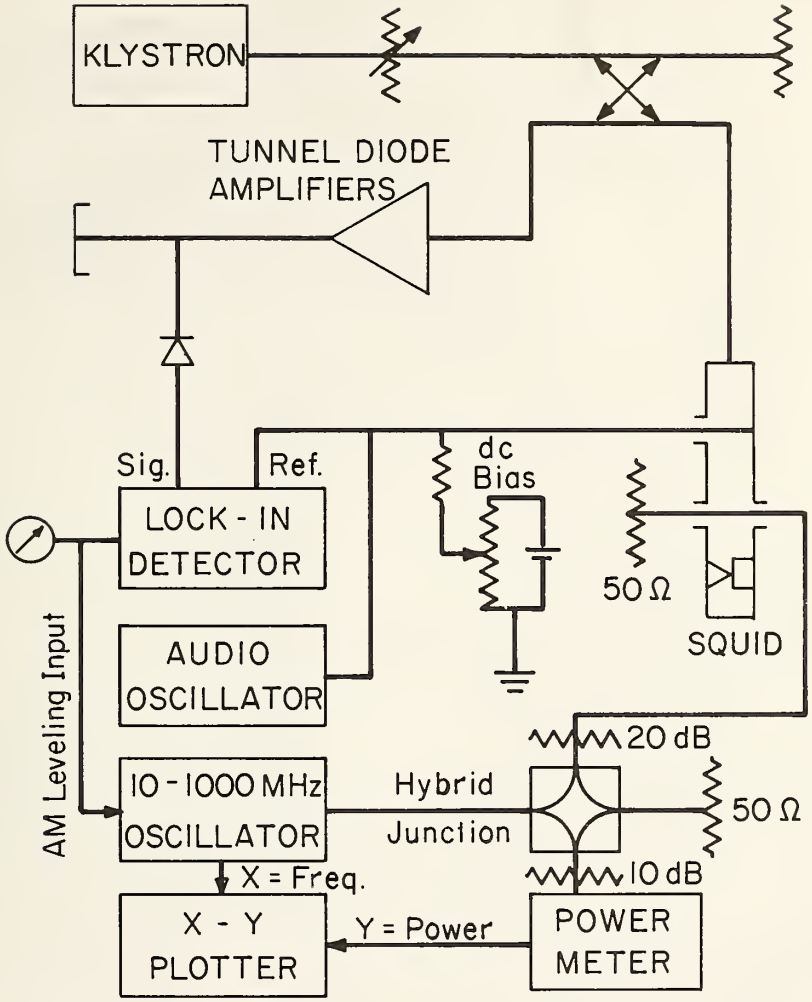


Figure 13. Arrangement for testing the frequency response of the system for measuring rf power.

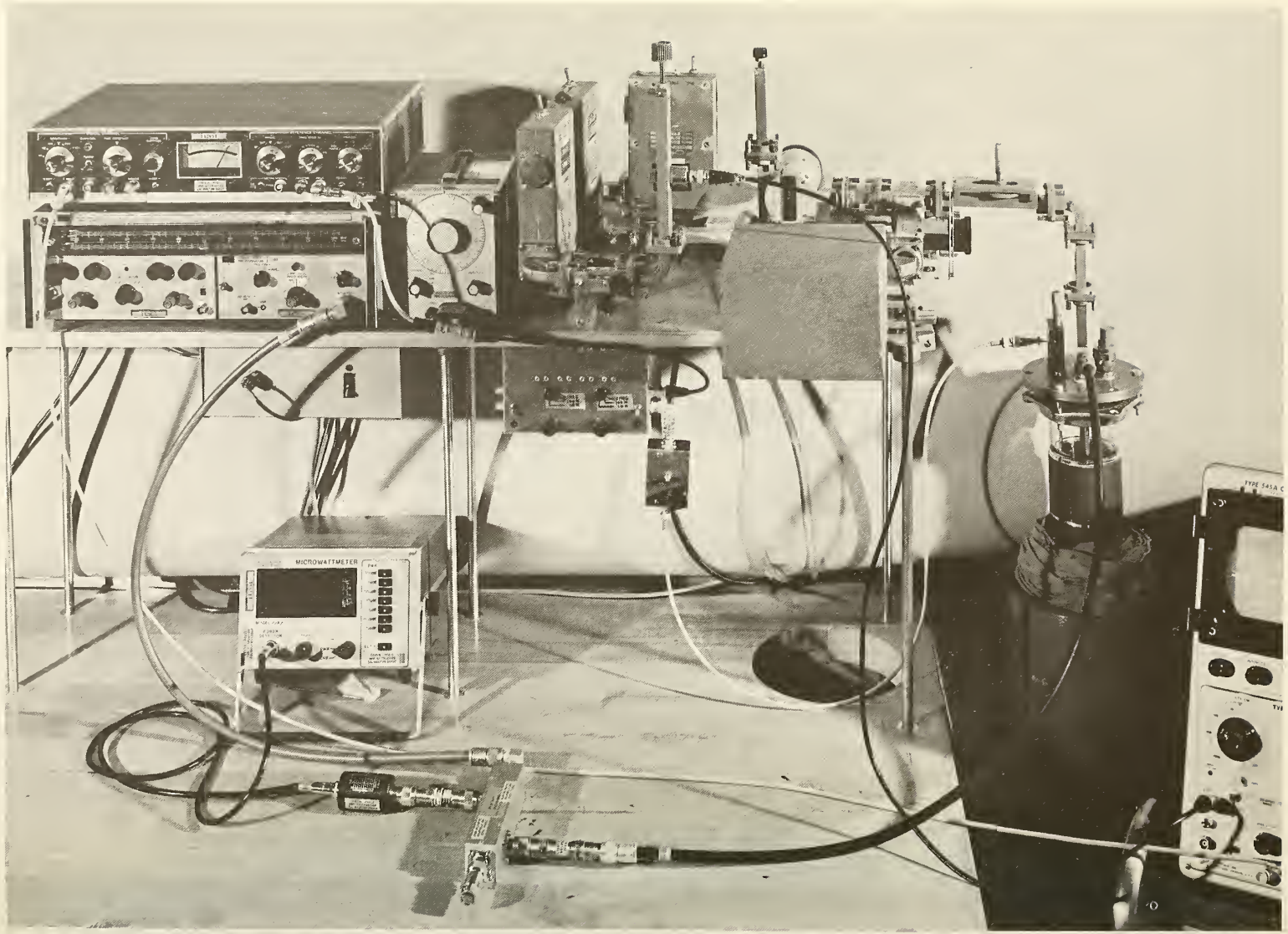


Figure 14. Realization of the system shown in figure 13.

modulation, which we used to control its output level with a servo loop using the SQUID as sensor. This had the effect of maintaining the rf current through the SQUID at a level corresponding to one of the nulls of its response as the frequency was swept from 10 MHz to 1 GHz. The result is shown in figure 15, which is a plot of the power registered by the bolometer versus frequency, drawn directly by an X-Y recorder. The smooth solid line superimposed on the chart recording shows the variation to be expected from the frequency dependence of the other components of the system if the current at the SQUID is assumed to be independent of frequency. The dashed curves on either side represent the approximate limits of error (± 1%) on the theoretical curve due to neglected small terms. Inspection of this figure shows that the assumption that the servo loop maintains a constant current at the SQUID, and hence that the calibration of the SQUID is independent of frequency, is supported by the experimental results within their limits of error (about ± 0.1 dB). The general rising trend of the curve is caused by the variation with frequency of the attenuation of the stainless steel coaxial lines connecting the SQUID with components outside the cryostat. It could be eliminated if a less lossy line were available.

At frequencies below 1 MHz the system becomes insensitive to reflections, and the rf current at the SQUID can be measured simply by connecting a voltmeter across the 50 Ω termination of the rf line. In this way we found the calibration constant $I_o$ (equation 7) to be constant at frequencies from 0 to 1 MHz and to have the same value from 10 MHz to 1 GHz within the uncertainty of the measurements (± 0.1 dB).

The SQUID we used for these tests had $I_o = 50$ μA. This placed the first null of its response at a power level of $10^{-8}$ W. As we mentioned in chapter 2, a modified version of this SQUID with the rf line closer to the Josephson junction had $I_o = 16$ μA. This would place the

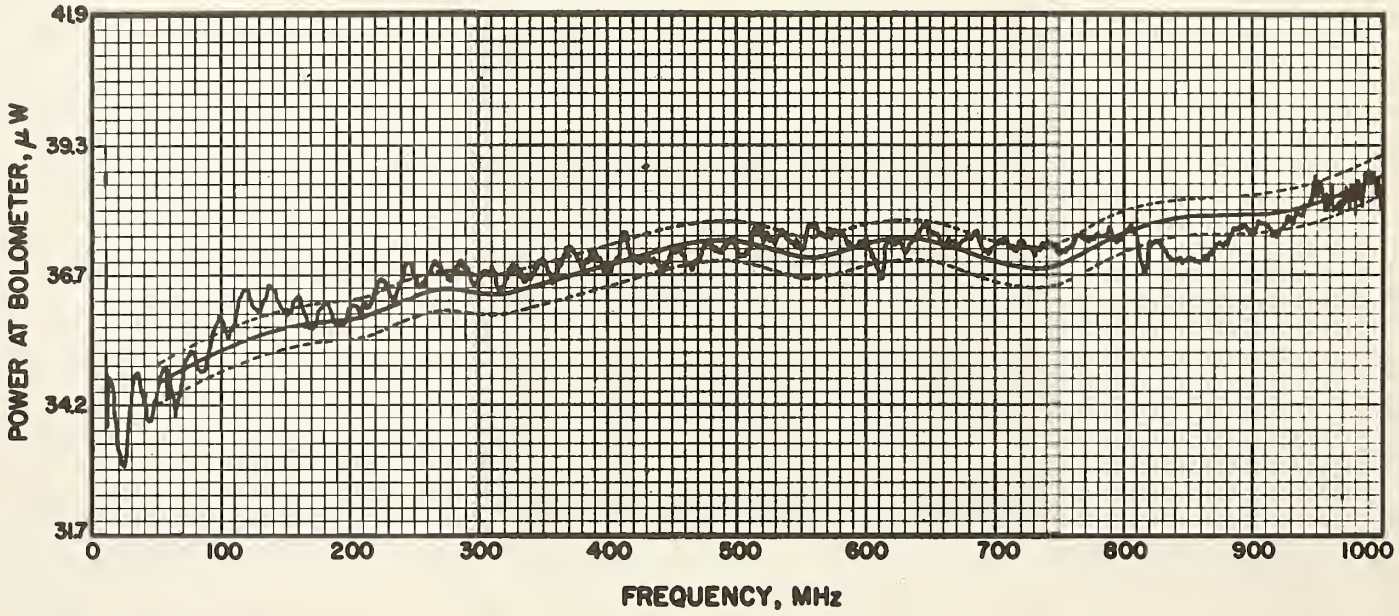


Figure 15. Swept-frequency display of power received by a bolometer from a generator levelled by a system using the SQUID for a reference. The solid curve superimposed on the recorder trace is the variation expected from the frequency dependence of the other components in the system. The dashed curves represent the limits of error (± 1%) expected in the theoretical curve from the neglect of small terms.

first null at $10^{-9}$ W. Using the first 100 nulls gives a dynamic range of about 45 dB above this level. The range of power accessible to measurement by the SQUID can be extended upwards by using attenuator pads. We have therefore shown that this system can measure power levels above one nanowatt with an uncertainty of $\pm$ 0.1 dB in the range of frequency from 0 to 1 GHz.

### 3.2 Power Levels Below One Nanowatt

Our strategy here calls for using a SQUID as a very sensitive indicator to compare the signal to be measured with a similar reference signal. For this role a readout system with a response to rf current of the form $J_o(2\pi I/I_o)$ is not acceptable. We need a response that rises linearly from zero for small current. Also, the broadband SQUID itself is not suitable, because the major part of the input power is dissipated in a passive load. For maximum sensitivity it must be dissipated in the Josephson junction itself. In this section we will describe the best forms we have found for the microwave readout system and the circuit to couple rf power to the SQUID. We will then sketch a complete system that could use these components for measuring power at very low levels.

We tried a variety of microwave readout systems before arriving at the one shown schematically in figure 16. It is essentially a heterodyne receiver which uses the SQUID as a mixer in the first stage. It is based on the simple system shown in figure 5. If a signal is applied to the SQUID from either the local oscillator or the rf input separately, then the voltage $\overline{V}$ at the first crystal detector has the form

$$\overline{V} = V_o + V_1 J_o(2\pi I/I_o)$$

where $I$ is the amplitude of the rf current at the appropriate port of the SQUID, and $I_o$ has different values at the two ports. To operate the

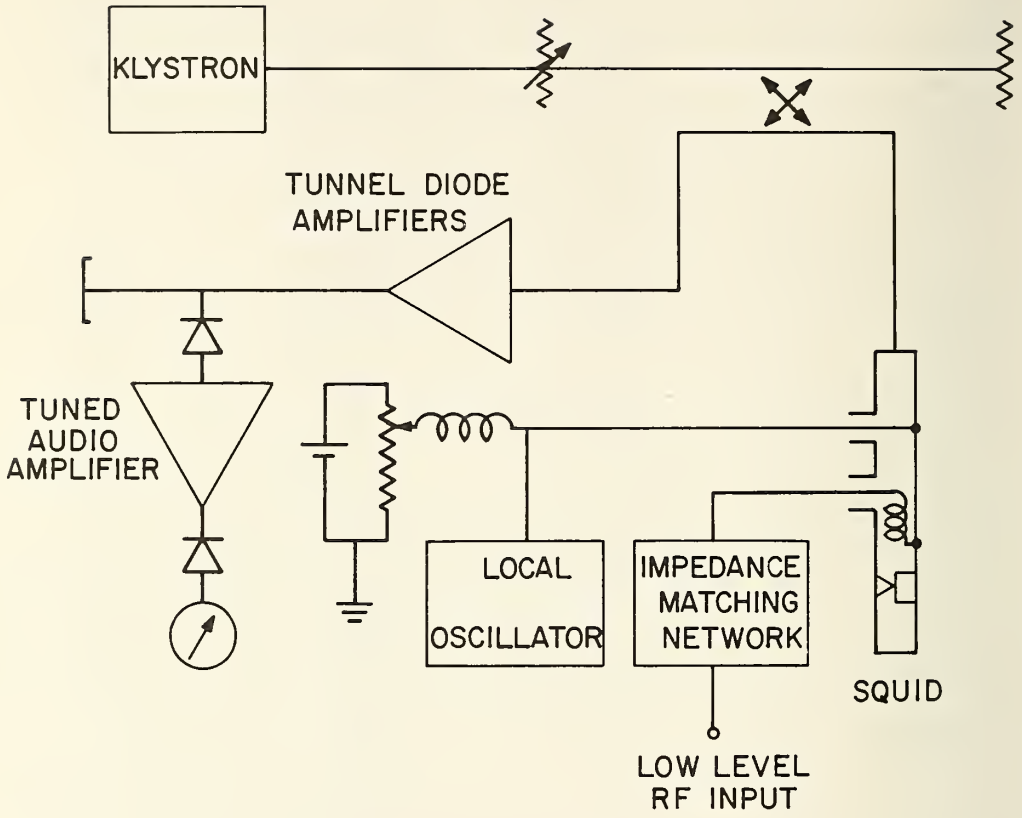


Figure 16. Detection system for measuring very low rf power levels.

system as a heterodyne receiver, we adjust the level of the local oscillator so as to bias the system to the first null of $J_o(2\pi I/I_o)$. At this point $\partial\overline{V}/\partial I$ has its maximum value. The weak incoming rf signal then mixes with the local oscillator to modulate the amplitude of the signal sensed by the SQUID at the difference frequency. This creates excursions of the reflected microwave signal about the null point of $J_o(2\pi I/I_o)$ at the difference frequency. The corresponding variations of $\overline{V}$ are amplified by an audio amplifier tuned to the difference frequency, rectified by a second detector, and displayed on a meter. The difference frequency must be chosen to lie within the post-detection bandwidth of the microwave system, which is limited to about 100 kHz by the first detector and the cable following it.

We found that this system can detect rf signals 40 dB below the level required to drive the SQUID to the first null of $J_o(2\pi I/I_o)$, with a time constant of 1 second at the meter. We could therefore use it to measure power with an uncertainty of $\pm$ 0.1 dB at a level 20 dB below this first null.

The objective, then, is to optimize the transfer of power to the SQUID by means of an impedance matching network. For this we have been using the SQUID with a toroidal coupling coil shown in figure 3. At frequencies below its self-resonance, this presents an inductive impedance, with a small resistive component to which the input circuit must be matched by balancing the inductance with a capacitive network. The result is a resonant circuit which matches the real impedance of the 50 $\Omega$ input line at a single frequency only. In order to cover a band of frequency, one can either broaden the resonance by using a complex network with interacting resonances, or use a simple tunable network with variable components.

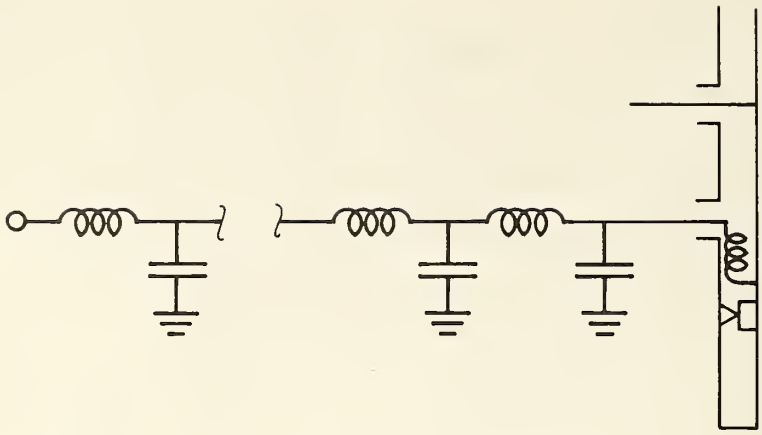

(a)

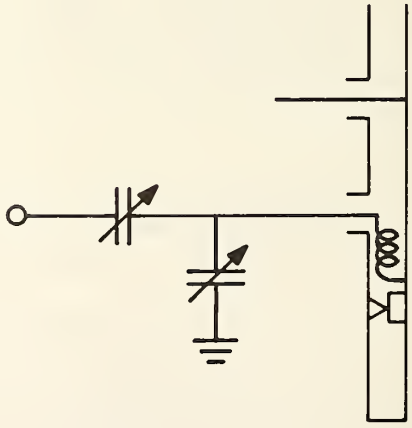

(b)

Figure 17. Impedance matching circuits: (a) bandpass; (b) tunable.

Networks with multiple resonances are used extensively as band-pass filters, and designs optimized with the aid of computers can be found in several handbooks [21]. We tried several of these with the basic form shown in figure 17a, using a SQUID with $I_o = 1.2$ μA. One of them, an asymmetric 5-pole Butterworth low-pass filter with a cutoff at 90 MHz, placed the first null of the response of the SQUID near $10^{-12}$ W over a range of frequency from 20 MHz to the limit of the test equipment we were using at 65 MHz. We would expect similar performance up to its cutoff frequency. The impedance it presented at its input was poorly matched to the 50 Ω line, so we tried a more ambitious 20-pole design which attempted to simulate a tapered section of waveguide. The characteristic impedance $\sqrt{L/C}$ was stepped logarithmically from stage to stage, from 50 Ω at the input to 1 Ω at the SQUID. All sections of the ladder were tuned to the same resonant frequency $1/(2\pi\sqrt{LC}) = 40$ MHz. This required a coupling coil in the SQUID of lower inductance with $I_o = 5$ μA. Its performance was similar to that of the simpler network. The first null of the response of the system was near $10^{-12}$ W at frequencies in the range from 9 MHz to 54 MHz, and the impedance matching was still very imperfect. A calculation with a computer suggested that this network should be capable of doing better. It probably requires tighter tolerances than we allowed on the values of the components.

The general conclusion is that it is feasible to make fixed networks covering ranges of about two octaves of frequency. Combined with the readout system we described earlier in this section, these would enable us to detect rf signals with a noise level of about $10^{-16}$ W.

In order to improve on this performance we tried the tunable network shown in figure 17b. It is a commonly used device, consisting of a capacitor in parallel with the inductor to form a circuit resonant at the operating frequency which is coupled to the input line through another capacitor adjusted for critical coupling.

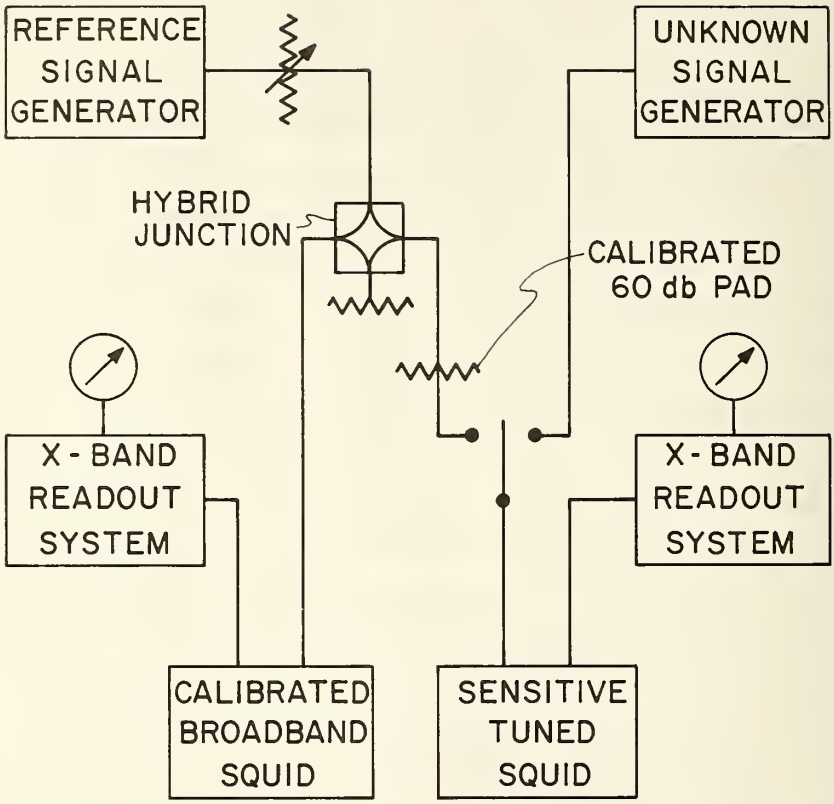


Figure 18. Proposed system for measuring low rf power levels (below $10^{-9}$ W).

To test this circuit we returned to the SQUID with a 50-turn coupling coil with $I_o = 1.2\ \mu A$. With a rather crudely connected circuit we obtained an essentially perfect match to the 50 Ω input line at frequencies in the range from 40 MHz to 65 MHz. On resonance, the first null of the response of the system was near $10^{-14}$ W. This would make the noise level of the system for detection of power about $10^{-18}$ W. The performance of this circuit can be improved by more careful placing and shielding of components. This would improve the tuning range by reducing stray inductance and improve the transfer of power by eliminating radiation loss.

The complete system we propose to use for measuring very low power levels is shown schematically in figure 18. The sensitive, tuned SQUID and its readout circuit will be used as an indicator, to compare the unknown signal with an identical reference signal. This latter will be prepared by using a reference oscillator tuned to the same frequency as the unknown signal. Power from the reference oscillator will be divided equally between two limbs by a hybrid junction. The first limb will pass to the system we described in the first part of this chapter for measuring high power levels (above one nanowatt). The second limb will pass through a calibrated 60 dB attenuator to become the reference signal. A variable attenuator in the reference line will be adjusted until the reference signal matches the unknown signal (as determined by the sensitive SQUID detector). The power level can then be determined by a measurement with the calibrated SQUID at a level 60 dB higher.

We are in the process of fabricating components to realize this scheme. We will aim to cover the range of frequency from 100 MHz to 1 GHz with the first model.

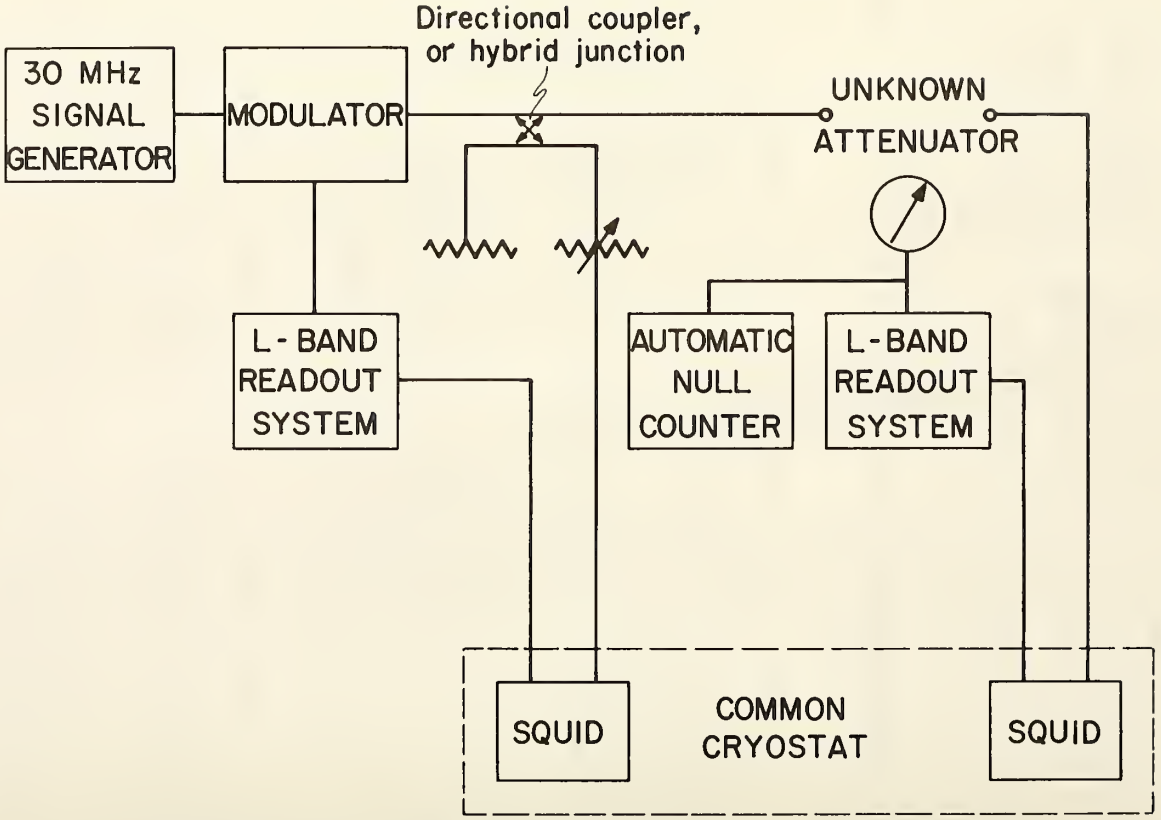


Figure 19. General layout of the system for routine calibration of attenuators.

# 4. MEASUREMENT OF ATTENUATION

The system we described in section 3.1 of this report can be used to measure variations in attenuation with no calibration whatever. A stable signal generator is connected to the SQUID via the variable attenuator under test. This can then be calibrated at the settings corresponding to the nulls of the response function $J_o(2\pi I/I_o)$. The ratio of the power levels at any pair of nulls can be calculated with the aid of a table of Bessel functions and compared with the difference between the two settings of the dial of the attenuator. The advantages of a standard of attenuation based on this principle are that the equipment is inexpensive and easy to fabricate (it requires no precise machining apart from standard commercial microwave components), and the system can be used at any frequency in the range from 0 to 1 GHz.

We demonstrated the feasibility of this technique some time ago [22]. As a second step, we have assembled a more specialized system based on the same principle, in order to gain experience with routine calibrations and also to explore the use of a readout system for the SQUID operating at L-band (1.2 GHz), to take advantage of less expensive components. This system was designed to measure attenuation at 30 MHz, and forms the subject of the remainder of this chapter.

## 4.1 The System

The general layout of the system is shown in figure 19. It uses two SQUIDs with independent readout systems. The first SQUID is the sensor in a servo loop to control the level of the signal at 30 MHz applied to the input of the attenuator under test. The second SQUID measures variations in the signal level at the output. The SQUIDs are identical and share a common cryostat. They are described in section 2.2 of this report (pages 19 - 23). The readout systems work on the same principle

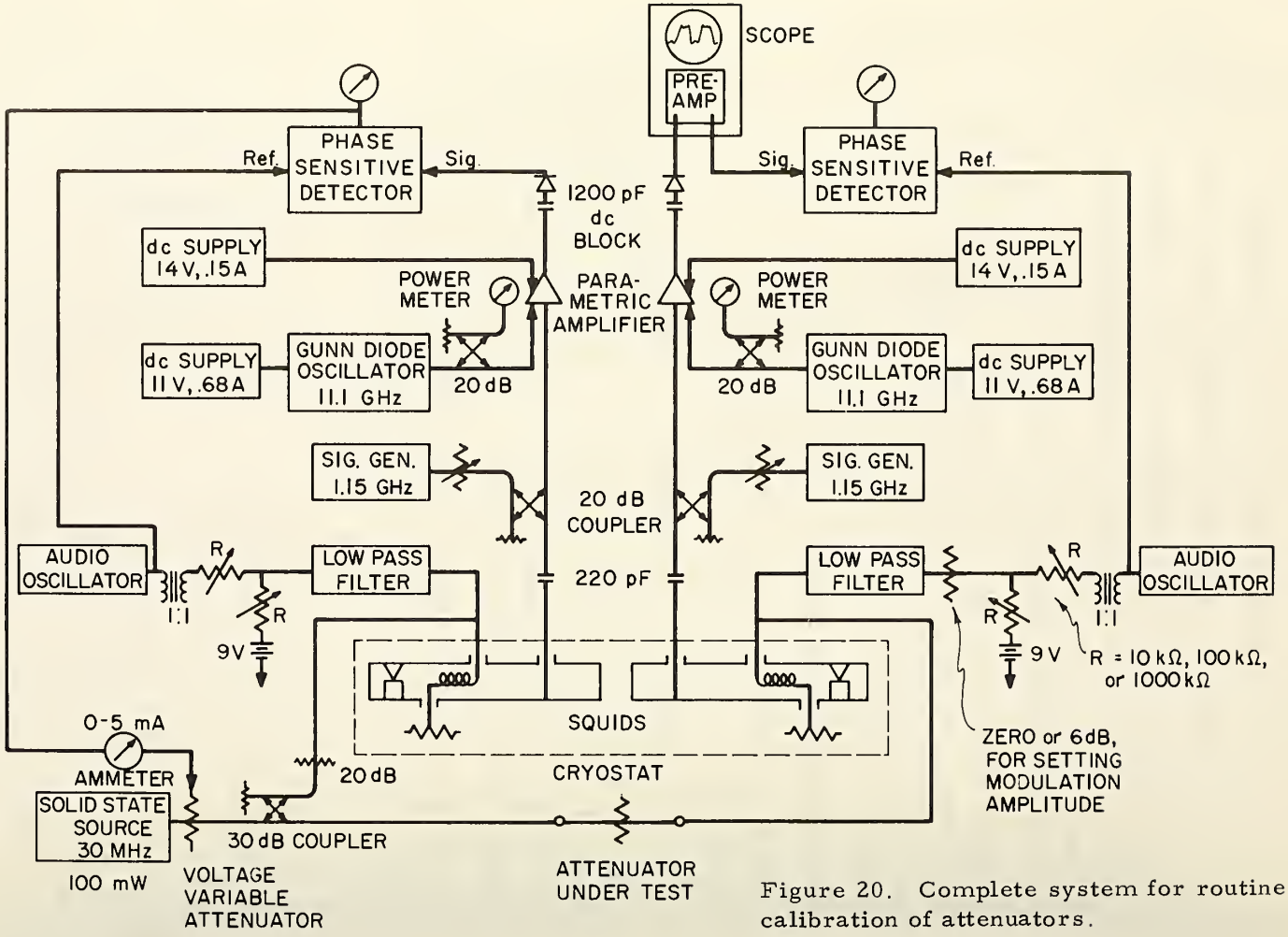


Figure 20. Complete system for routine calibration of attenuators.

as the one shown in figure 11, with trivial changes in the coupling of signals to the SQUIDs. The voltage at the meter of each lock-in detector is a function $J_o(2\pi I/I_o)$ of the amplitude I of the rf current at the corresponding SQUID. In the stabilizing circuit this voltage is applied to a modulator (voltage-variable attenuator) in the rf line. It controls the level of rf power so as to remain locked to any chosen null of the function $J_o(2\pi I/I_o)$, compensating for variations in the level of the signal generator by applying equal and opposite variations to the attenuation of the modulator. In the measuring circuit the meter on the lock-in detector is used to locate the nulls of the response function $J_o(2\pi I/I_o)$ as the attenuator under test is adjusted. The system is set on a sequence of these nulls, and the reading of the attenuator dial is noted at each null. The dial readings are then compared with attenuation ratios calculated with a table of Bessel functions.

Figure 20 shows more details of the components we used to realize this system. The microwave systems are driven by L-band signal generators delivering a few nanowatts of power to the 20 dB directional couplers. The power level at the SQUIDs is therefore of order $10^{-11}$ W. The reflected microwave signals are amplified by parametric amplifiers pumped by Gunn diode oscillators operating at X-band. The parametric amplifiers are followed by several stages of amplification by transistors to give a total gain of about 50 dB. It is not necessary to use such expensive amplifiers: we happened to possess some surplus units which we used for this project. Quite inexpensive transistor amplifiers are available with adequate performance. After amplification, the microwave signals are rectified by crystal diodes. The signals at these points are at a level of a few mV. They are applied to the lock-in detectors, which have their own internal preamplifiers to raise the signals to their operating levels of a few volts. We insert an oscilloscope in the circuit for

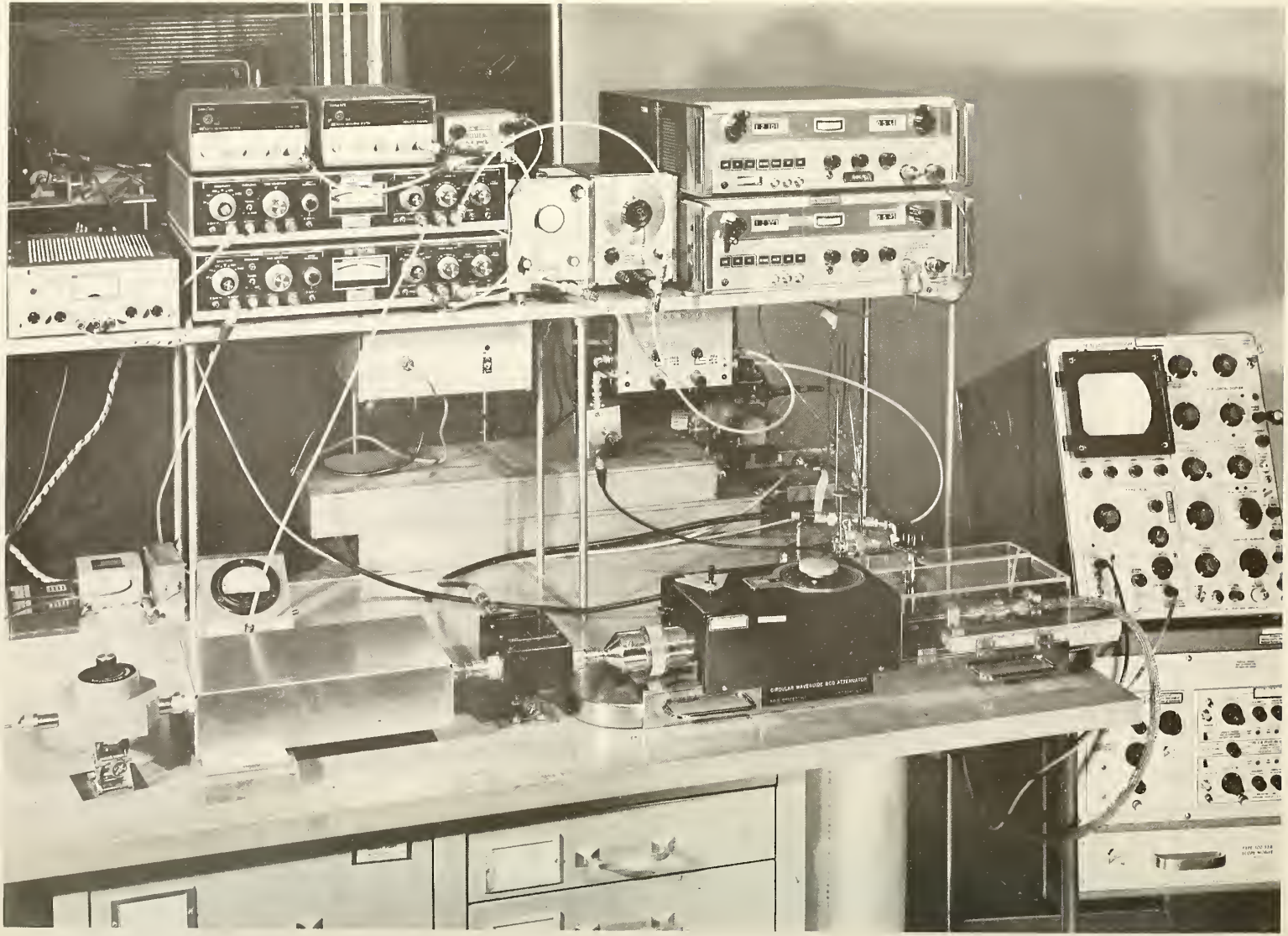


Figure 21. Realization of the system shown in figures 19 and 20.

the measuring SQUID to monitor its levels of bias and modulation. The modulation frequency is 1 kHz. We supply modulation and dc bias to the SQUIDs via low-pass filters connected to the rf lines. These must pass the bias and modulation, but must present a high impedance (to avoid loading) and at least 60 dB of attenuation to signals at 30 MHz. The high degree of attenuation is required to prevent cross-talk between the stabilizing and measuring channels: some of the low-frequency components are mounted in common boxes, which present a possible path by-passing the attenuator under test. Bias and modulation levels are of the order of $10^{-3}$ V at the SQUIDs.

The source of the signal at 30 MHz is a very stable crystal-controlled solid state oscillator. It delivers 100 mW, and we have an amplifier of comparable stability available to raise this level to the maximum permitted by the attenuator under test. The voltage variable attenuator has a range from 0 to 20 dB as the bias current varies from 0 to 3 mA respectively. We can obtain a greater range if necessary by connecting several modulators in series. All connections are either semi-rigid coaxial line (with solid conductors) or double-screened flexible coaxial line (with braided conductors). With this precaution and some care with connectors, leakage does not appear to be a significant problem. Figure 21 shows the completed system.

The cryostat is made of glass, with two copper radiation shields in the vacuum space between the inner and outer walls. These shields are attached to the inner wall near the neck, so that the escaping helium gas cools them. The interstices between them and the walls are filled with several layers of aluminized polyester film, for additional radiation baffles. No liquid nitrogen is required. Starting with a warm system, about 2 liters of liquid helium are required for the initial cooldown and a day's running.

This cryostat has been described in the literature by Zimmerman and Siegwarth [1], its designers. It will shortly be replaced by their more advanced version made of an epoxy-fiberglass composite. We expect these to retain the liquid helium for a longer period, since they are longer, and have five radiation shields.

## 4.2 Operation

We will show in the following section that this system is capable of matching the accuracy of any other method of measuring attenuation at 30 MHz. However, achieving this accuracy requires careful attention to setting up the optimum operating conditions.

The basic source of systematic error is a deviation of the response of the SQUID and its readout circuit to rf current I from the simple form $J_o(2\pi I/I_o)$. This in turn is caused by harmonic distortion of the simple sinusoidal response of the system to direct current. We will analyze this in detail in chapter 5. We will show that this distortion affects the positions of the first few nulls of the response function much more strongly (measured in dB) than those of higher order. The magnitude and direction of these errors depend upon the setting of the dc bias and the depth of modulation at the SQUID. The effect of the lowest order of distortion (second harmonic) can be cancelled out exactly for all nulls by setting the dc bias at a point of symmetry (one of the peaks or valleys of figure 1a), or by setting the amplitude $I_m$ of the modulating current so that $J_1(4\pi I_m/I_o) = 0$.

To set these conditions in practice, we note that the component of the readout signal picked out by the lock-in detector is proportional to $J_1(2\pi I_m/I_o)$. With the system running, we adjust the modulating current until the lock-in detector indicates the first null, so that $J_1(2\pi I_m/I_o) = 0$. We then insert 6 dB of attenuation in the modulation supply to halve the

modulating current. Then $J_1(4\pi I_m/I_o) = 0$. Looking at the oscilloscope, we then adjust the dc bias until the trace appears symmetrical.

We usually make these adjustments with the signal at 30 MHz turned off. During measurements of attenuation, this signal is present at a varying power level which can exceed that of the microwave readout signal. We have occasionally observed systematic errors at high power levels caused by mixing of: the rf signal; the microwave readout signal; and the dc bias, by the highly nonlinear properties of the SQUID. The result is that the optimum settings of the bias and modulation become power-dependent, an intolerable situation. A symptom of this problem is that the average reflected microwave signal (ignoring the structure due to quantum interference) varies with changes in the power level at 30 MHz. Before making measurements, we adjust the Josephson junction to suppress this effect. In general, a rather weak contact (low critical current $I_c$ ) is best.

These errors were dramatically reduced when we replaced the simple point contact junctions (between bare niobium screws) in the SQUIDs by the plated and spring-loaded contacts described in section 2.3 of this report. Apart from their mechanical stability, these behave electrically like simple point contacts shunted by small resistors. This suppresses the mixing of signals and also reduces the harmonic distortion of the response of these SQUIDs, which is the basic cause of most of the errors. All our best results have been obtained with these improved contacts.

There are some residual problems with noise and drift. These appear to vary at random from day to day. Further work will be required to get them fully under control. Also, the circuit to stabilize the rf level at the input of the attenuator under test appears to increase the noise level in the system when it is operating. We will need to shape its

TABLE 1: Basic Program to Analyze Data

```
5  REM TABLE OF ZEROS FOR JO
10 DIM J(100),D(100),Z(100),M(100)
20 Z(1) = 53.57201
30 READ J(1)
31 FOR I=2 TO 100
32 READ J(I)
34 Z(I) = 20*LGT(J(I)/J(1))
37 Z(I) = Z(1) -Z(I)
40 NEXT I
42 PRINT
44 PRINT" I      THEORY     MEASURED          T-M"
50 FOR I=1 TO 100
60 READ M(I)
65 IF M(I) = 0 THEN 80
70 PRINT I ;Z(I);M(I),Z(I)-M(I)
80 NEXT I
200 DATA 2.40483,5.52008,8.65373,11.79153,14.93092
202 DATA 18.07106,21.21164,24.35247,27.49348,30.63461
204 DATA 33.77582,36.91710,40.05843,43.19979,46.34119
206 DATA 49.48261,52.62405,55.76551,58.90698,62.04847
208 DATA 65.18996,68.33147,71.47298,74.61450,77.75603
210 DATA 80.89756,84.03909,87.18063,90.32217,93.46372
212 DATA 96.60527,99.74682,102.88837,106.02993,109.17149
214 DATA 112.31305,115.45461,118.59618,121.73774,124.87931
216 DATA 128.02088,131.16245,134.30402,137.44559,140.58716
218 DATA 143.72873,146.87031,150.01188,153.15345,156.29503
220 DATA 159.43661,162.57819,165.71977,168.86135,172.00292
222 DATA 175.14450,178.28608,181.42766,184.56924,187.71083
224 DATA 190.85241,193.99309,197.13557,200.27716,203.41874
226 DATA 206.56032,209.70191,212.84349,215.98507,219.12666
228 DATA 222.26824,225.40983,228.55141,231.69300,234.83458
230 DATA 237.97617,241.11775,244.25934,247.40093,250.54251
232 DATA 253.68409,256.82569,259.96727,263.10886,266.25045
234 DATA 269.39203,272.53362,275.67520,278.81680,281.95838
236 DATA 285.09997,288.24156,291.38315,294.52473,297.66632
238 DATA 300.80791,303.94950,307.09109,310.23268,313.37427
300 DATA 53.572,46.361,42.447,39.763,37.712,36.057
310 DATA 34.664,33.464,32.409,31.470,0,29.850,0,0,27.874
320 DATA 0,0,0,0,25.339,0,0,0,0,23.380,0,0,0,0,21.781
330 DATA 0,0,0,0,0,0,0,0,0,19.263
340 DATA 0,0,0,0,0,0,0,0,0,17.315
350 DATA 0,0,0,0,0,0,0,0,0,15.722
360 DATA 0,0,0,0,0,0,0,0,0,0,0,0,0,0,0,0,0,0,13.216
370 DATA 0,0,0,0,0,0,0,0,0,0,0,0,0,0,0,0,0,0,11.272
```

frequency response more carefully to improve its performance. Fortunately, the 30 MHz signal generator we are using is sufficiently stable so that its fluctuations do not limit the present accuracy of our measurements even without a stabilizing circuit. We obtained our best results so far with the signal generator running free.

Our procedure for calibrating an attenuator is to note the readings on its dial corresponding to a sequence of nulls of the response of the second SQUID. We use a simple computer program (in "basic" language) to compare these readings with attenuation ratios calculated from a table of Bessel functions and to print out the deviations. Table 1 is a listing of this program. Lines 5 - 80 are the program itself; line 20 is an arbitrary number representing the insertion loss; lines 200 - 238 are the arguments of the first 100 zeros of the Bessel function $J_o$; lines 300 - 370 are attenuator dial settings from a typical experimental run. In order to keep track of order numbers, we record "0" for nulls that we skip. Table 2 shows the form in which the computer prints out the results of its calculation. From these data it is convenient to plot a calibration curve (deviation versus dial reading), such as we will discuss in the following section.

### 4.3 Results

For testing this system we used an NBS Model VII piston attenuator. This was first calibrated by the NBS Calibration Service, and then used in a series of tests with the new system using SQUIDs.

During these tests we encountered, and partially solved or avoided, all the problems we mentioned in the previous section of this report. Finally, when everything was running well, we were able to obtain results such as those illustrated in figure 22. This is a plot of deviation versus dial setting for the piston attenuator, representing the results of

TABLE 2: Results of a Typical Run

RUN

| I | THEORY | MEASURED | T-M |
|---|---|---|---|
| 1 | 53.57201 | 53.572 | .0999984E-04 |
| 2 | 46.35479 | 46.361 | -.6209814E-02 |
| 3 | 42.44963 | 42.447 | .2630803E-02 |
| 4 | 39.76229 | 39.763 | -.0705583E-02 |
| 5 | 37.71197 | 37.712 | -.337488E-04 |
| 6 | 36.05403 | 36.057 | -.2974935E-02 |
| 7 | 34.66221 | 34.664 | -.1787334E-02 |
| 8 | 33.46284 | 33.464 | -.1162719E-02 |
| 9 | 32.4091 | 32.409 | .1033339E-03 |
| 10 | 31.46945 | 31.47 | -.5494959E-03 |
| 12 | 29.84915 | 29.85 | -.0853938E-02 |
| 15 | 27.87435 | 27.874 | .3539839E-03 |
| 20 | 25.33908 | 25.339 | .0760788E-03 |
| 25 | 23.37932 | 23.38 | -.0983951E-02 |
| 30 | 21.78084 | 21.781 | -.163631E-03 |
| 40 | 19.26389 | 19.263 | .0887811E-02 |
| 50 | 17.31479 | 17.315 | -.2057422E-03 |
| 60 | 15.72391 | 15.722 | .1911021E-02 |
| 80 | 13.21607 | 13.216 | .06914E-03 |
| 100 | 11.27243 | 11.272 | .4309156E-03 |

>

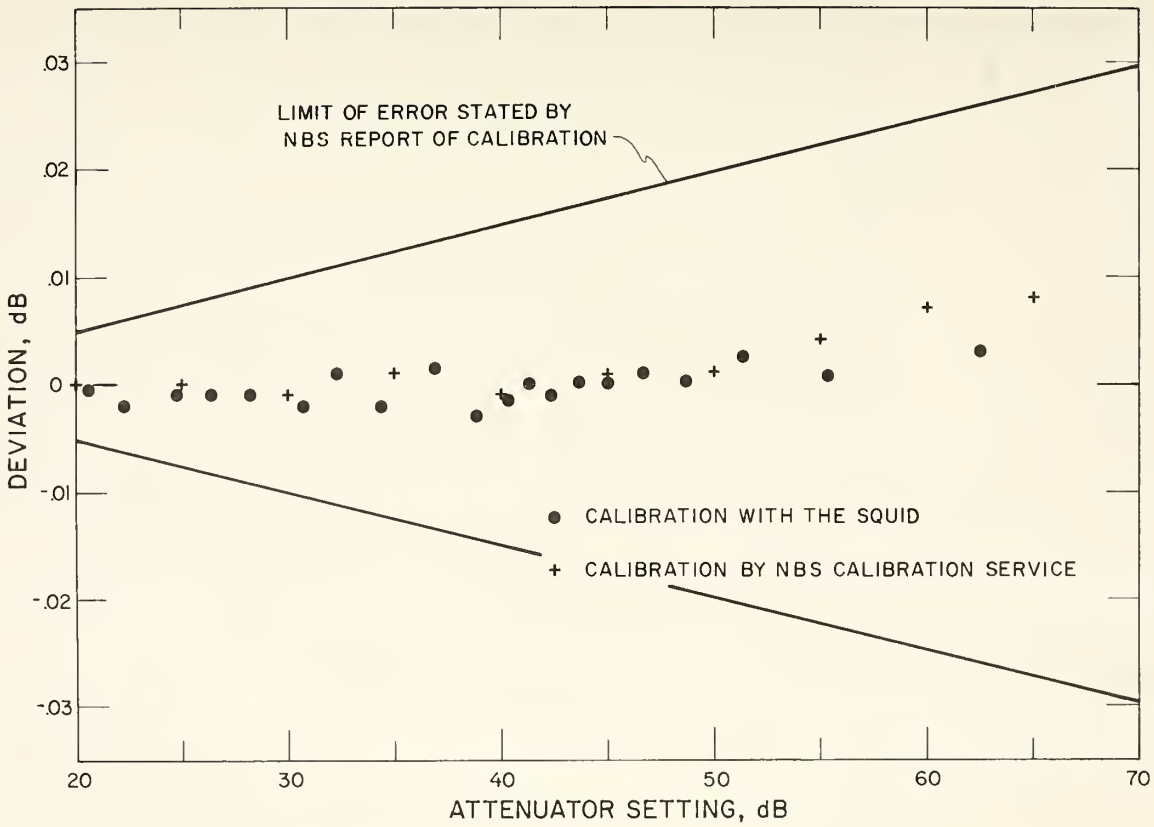


Figure 22. Comparison of a calibration of a variable attenuator using the SQUID system (dots) with the NBS calibration service (crosses). The solid lines represent the estimated limits of error written on a typical report of calibration.

a single run with the SQUID. The dots represent measurements made with the SQUID, while the crosses at 5 dB intervals represent the information supplied by the NBS Calibration Service. The limits of error normally written on a report of calibration [23], to cover random and possible systematic errors, are represented by the diverging lines. Each cross represents the average of three measurements, while each dot represents a single measurement.

The average rms deviation of the three measurements at each point taken by the NBS Calibration Service was ± 0.0011 dB. The rms deviation of the measurements taken with the SQUID from a smooth curve drawn through the calibration points was ± 0.0017 dB, the major contribution coming from the last two points at high attenuation. These correspond to the first and second nulls of the response of the SQUID, which are the most prone to errors due to harmonic distortion. On the other hand, the power level in the NBS calibrating system is raised at 50 dB to a higher level for measuring high attenuation. This is known to increase the systematic error in the range above 50 dB. Apart from these considerations based on previous knowledge of the idiosyncrasies of the two systems, the difference in scatter between the two sets of measurements is not statistically significant in such a small number of samples.

The most obvious feature of figure 22 is the large discrepancy between the estimated limits of the systematic error of the NBS calibration and the degree of agreement between the two entirely independent methods of measuring attenuation. Clearly, the estimated errors are very conservative, but so long as one accepts them it is difficult to say which system is testing which. We hope that after further careful comparison of measurements made by the two systems it will be possible to revise the estimate of errors and issue reports of calibration giving better justice to the quality of the measurements that are actually made.

The first fruit of developing the new system will therefore be to demonstrate the full extent of the virtues of the old one. The new system also has the inherent advantages that it is cheaper to construct and covers a wide range of frequency. We believe that when it is fully developed it will be a strong contender for the position of primary standard of attenuation.

# 5. SYSTEMATIC ERRORS

In this chapter we consider two sources of systematic error in measurements of rf current by the techniques we have described. These are variation with frequency of the geometrical factor relating current in the rf circuit to magnetic flux linking the SQUID, and distortion of the basic scale defined by the nulls of the function $J_o(2\pi I/I_o)$. We will dismiss the first of these topics with a few estimates of orders of magnitude: it is not a serious source of error, it affects measurement of absolute power but not attenuation, and it is well understood by microwave circuit designers. Since the second topic is unique to our new measuring system, we will analyze it in some detail.

## 5.1 The Geometrical Factor

The two effects to consider are: the variation with frequency of the depth of penetration of current into the conducting walls of the SQUID, with the consequent variation in the distribution of current; and the variation with frequency of the distribution of electromagnetic fields in the hollow spaces of the SQUID because of the formation of standing waves.

The penetration depth for current into the surfaces of superconducting lead and niobium (the two materials we most commonly use for SQUIDs) is about $4 \times 10^{-8}$ m. This quantity varies slightly with frequency. Waldram [24] found that the penetration depth in tin changes by 8% between dc and 9.4 GHz. One would expect lead and niobium to be less sensitive to frequency, but a change of 8% would amount to $3 \times 10^{-9}$ m. The smallest linear dimension of any SQUID we have made so far is $2.5 \times 10^{-4}$ m, so the effective linear dimensions of the superconducting walls of the SQUID might change by 10 parts per million between dc and X-band. We can neglect this for present purposes.

The presence of standing waves will cause a significant perturbation of the distribution of electromagnetic fields inside a hollow conductor when the wavelength is comparable to the linear dimensions of the conductor. For smaller conductors, the perturbation will be of the order of $1 - \cos(\ell/\lambda)$ where $\ell$ is the longest linear dimension and $\lambda$ the wavelength. Integrating this over the length of one of the simple X-band SQUIDs (figure 2), which we use to measure high levels of power, yields an error of one part per thousand at 1 GHz. SQUIDs coupled to the rf line by coils (see figures 3 and 6) are affected by standing waves at much lower frequencies, because they are slow-wave structures. However, our mode of using them does not rely on their calibration being independent of frequency.

## 5.2 Distortion of the Basic Scale

The microwave SQUID, together with its microwave readout system, converts variations in magnetic flux $\varphi$ (induced by current I in the coaxial input line) to variations in an output voltage V which depends periodically on $\varphi$. The functional form is very nearly sinusoidal:

$$V = V_o + V_1 \cos(2\pi I/I_o)$$

$$= V_o + V_1 \cos(2\pi \varphi/\varphi_o) \qquad (9)$$

where $I_o$ is the increment of current required to change $\varphi$ by one flux quantum $\varphi_o$. Faced with current alternating at a radio frequency $f_{rf}$, we assume that the recording system would register an average value $\overline{V}$ of the output voltage V. In the approximation that the basic response to current (eq. 9) is sinusoidal, we will see that

$$\overline{V} = V_o + V_1 J_o(X_o) \qquad (10)$$

where

$$I = \frac{X_o I_o}{2\pi} \cdot \sin(2\pi f_{rf} t).$$

With some technique to locate the zeros of $J_o(X_o)$ the system is then capable of measuring ratios of rf current and hence power. Equations (9) and (10) represent such a close approximation to the observed performance of the system that we can regard them as "normal." Any deviation is an "error" to be analyzed and corrected.

We observe that the system always appears to respond symmetrically to increasing and decreasing magnetic flux. We may therefore represent the basic response with a Fourier cosine series

$$V = V_o + \sum_n V_n \cos(nX + n\delta) \qquad (11)$$

where $X = 2\pi I_{rf}/I_o = X_o \sin(2\pi f_{rf} t)$. It represents the rf current in units of the flux quantum. The quantity $\delta$ is defined in a similar way to include contributions to the input current (such as dc bias and low frequency modulation) which vary with time much more slowly than the rf current (slowly enough for the recorder to follow). Expanding the cosines in equation (11):

$$V = V_o + \sum_n \left[ V_n \cdot \cos(nX) \cdot \cos(n\delta) - V_n \cdot \sin(nX) \cdot \sin(n\delta) \right] \qquad (12)$$

and integrating over a complete rf cycle:

$$\overline{V} = V_o + \sum_n \left[ \left( V_n \cos(n\delta)/2\pi \right) \int_o^{2\pi} \cos(nX_o \sin y)\, dy \right.$$

$$\left. - \left( V_n \sin(n\delta)/2\pi \right) \int_o^{2\pi} \sin(nX_o \sin y)\, dy \right] \qquad (13)$$

where $y = 2\pi f_{rf} t$. The second term in the square brackets vanishes on integration, and the first term is Bessel's original expression for $J_o$. Hence

$$\overline{V} = V_o + \sum_n 2V_n \cdot \cos(n\delta) \cdot J_o(nX_o). \qquad (14)$$

We now fill in more detail in $\delta$, which includes both dc bias and low frequency modulation.

$$\delta = a + b \sin(2\pi f_M t) \qquad (15)$$

$$= a + b \sin z$$

where: $a = 2\pi I_{dc}/I_o$; $b = 2\pi I_M/I_o$. $I_{dc}$ is the dc bias and $I_M$ is the depth of modulation at frequency $f_M$. The modulated signal $V_M \sin z$ at the output of the microwave system may then be used with a lock-in detector to locate the zeros of the Bessel function part of the response expressed in equation (14). The quantity $V_M$ is the first Fourier coefficient of $\overline{V}$:

$$V_M = \frac{1}{\pi} \int_{-\pi}^{\pi} \overline{V} \cdot \sin z \cdot dz \qquad (16)$$

using equation (14):

$$V_M = \frac{1}{\pi} \sum_n V_n \cdot J_o(nX_o) \int_{-\pi}^{\pi} \sin z \cdot \cos(na + nb \cdot \sin z) \cdot dz \qquad (17)$$

expanding the cosines:

$$V_M = \frac{1}{\pi} \sum_n V_n \cdot J_o(nX_o) \cdot \int_{-\pi}^{\pi} \Big[ \cos(na) \cdot \cos(nb \cdot \sin z) \cdot \sin z - \sin(na) \cdot \sin(nb \cdot \sin z) \cdot \sin z \Big] dz. \qquad (18)$$

The first term in the square brackets vanishes on integration, leaving:

$$V_M = -\frac{1}{\pi} \sum_n V_n J_o(nX_o) \cdot \sin(na) \int_{-\pi}^{\pi} \sin(nb \cdot \sin z) \sin z \cdot dz \qquad (19)$$

or

$$V_M = \sum_n 2V_n \cdot J_o(nX_o) \cdot \sin(na) \cdot J_1(nb). \qquad (20)$$

The quantity $V_M$ in equation (20) is the signal that would be recorded by a lock-in detector following the microwave crystal detector, with reference at the modulation frequency. The approximate form of this signal given in equation (10) corresponds to the leading term of equation (20) with $n = 1$. The other terms distort this signal by adding Bessel functions of multiple argument.

Let us consider the simplest case, where only second harmonic distortion of the basic response occurs ($n = 1, 2$):

$$V_M = 2V_1 \cdot \sin(a) \cdot J_1(b) \cdot J_o(X_o) + 2V_2 \cdot \sin(2a) \cdot J_1(2b) \cdot J_o(2X_o). \qquad (21)$$

The presence of the second term shifts the zeros from where they would be with the first term alone. In order to find where they get to, let us consider the function:

$$V_M/2V_1 \sin(a) \cdot J_1(B) = J_o(X_o) + \alpha J_o(2X_o) \tag{22}$$

where

$$\alpha = \left[V_2 \cdot \sin(2a) \cdot J_1(2b)\right] \Big/ \left[V_1 \cdot \sin(a) \cdot J_1(b)\right].$$

Neglecting second derivatives, a simple analysis shows that the zeros of the function in equation (22) occur at

$$X_o = j_o + \Delta X$$

where

$$\Delta X = \alpha J_o(2j_o) \Big/ \left[J_1(j_o) + 2\alpha J_1(2j_o)\right] \tag{23}$$

and

$$J_o(j_o) = 0,$$

i.e.: $j_o$ is the argument of the Bessel function at the unperturbed zero.

If $2\alpha \ll 1$, we can neglect the second term in the square brackets, and

$$\Delta X \approx \alpha J_o(2j_o)/J_1(j_o).$$

Table 3 gives the numbers required to calculate the perturbation of the first ten zeros.

TABLE 3: Numerical values of quantities in equation (23), for calculating the effect of second harmonic distortion.

| Zero Number | $J_o(2j_o)$ | $J_1(j_o)$ | $J_1(2j_o)$ | $J_o(2j_o)/J_1(j_o)$ |
|---|---|---|---|---|
| 1 | -0.2374 | +0.5191 | -0.300 | -0.46 |
| 2 | -0.1640 | -0.3403 | -0.183 | +0.48 |
| 3 | -0.1327 | +0.2715 | -0.142 | -0.49 |
| 4 | -0.1143 | -0.2325 | -0.120 | +0.49 |
| 5 | -0.1019 | +0.2065 | -0.106 | -0.49 |
| 6 | -0.0919 | -0.1877 | -0.096 | +0.49 |
| 7 | -0.0858 | +0.1733 | -0.088 | -0.50 |
| 8 | -0.0802 | -0.1617 | -0.082 | +0.50 |
| 9 | -0.0755 | +0.1522 | -0.077 | -0.50 |
| 10 | -0.0716 | -0.1442 | -0.073 | +0.50 |

Inspection of this table reveals several interesting points:

1) If $2\alpha \ll 1$, the odd and even zeros are shifted by equal amounts in opposite directions. (This is true only for second harmonic distortion. The third harmonic moves odd and even zeros in the same direction.) The amount $\Delta X$ tends to a constant value after the first few zeros. The error in dB on measurement of a ratio would be $20 \log_{10}(1 + \Delta X/j_o)$, which is greatest for the first zero and diminishes for zeros of higher order.

2) A shift of 0.1 dB in the position of the first zero implies $\alpha = 0.055$ (second harmonic 25 dB down).

3) If $2\alpha$ becomes large enough to be significant compared with unity, the second term under the square brackets in equation (23) has the effect of making the errors in the odd zeros larger, and the errors in the even zeros relatively smaller.

4) Going back to equation (22), we see that the sign and magnitude of $\alpha$ depends upon both the dc bias, a, and the depth of modulation, b. The error can be nulled out for all zeros by adjustment of either or both of these quantities. It so happens that the settings of a and b that null out the errors are also just those which peak up the desired signal.

5) This happy state of affairs is modified somewhat by the presence of the higher order terms $(n > 2)$ in equation (20). Assuming that these contribute only a small part of the error, it should still be possible to minimize the errors by choosing the proper setting of a and b. This will probably no longer null out the errors in all the zeros simultaneously, but usually only the errors in the first few zeros are significant. The optimum settings of a and b will probably be displaced from the values suggested by equation (22).

6) The errors we have been discussing only occur when the basic response of the system is distorted from the sinusoidal form. Some effort to avoid this has proved fruitful.

In summary, errors are introduced into the basic scale by harmonic distortion, but the error can be minimized by proper choice of modulation depth and bias level. Second harmonic distortion causes the odd and even points to split apart into two branches with opposite errors. Third harmonic distortion causes errors with the same sign for both.

# 6. OBVIOUS IMPROVEMENTS

This chapter is a potpourri of ideas for improving the technique, described in chapter 4 of this report, for using a SQUID for measuring rf attenuation. We have tried "breadboard" models of some of them, but they will all require further development before we incorporate them in a proper working system.

## 6.1 Automatic Counting of Nulls

The form of the signal at the lock-in detectors in the readout circuits for the SQUIDs (figures 11 and 20) is suitable (with some attention to noise) for driving a counter. In order to record usable information, the counter must be arranged to count the number of nulls lying between the power level at the SQUID and zero power.

The most convenient device to accomplish this would be an up-down counter, which senses whether the power level is rising or falling and adds or subtracts counts accordingly. This requires two signals to drive it. Both must have periodic positive and negative excursions, and the peaks of one signal must coincide with the nulls of the other. The counter can then sense whether a given null in the first signal is on the high or the low side of the previous peak by referring to the sign of the second signal.

We tried to derive a suitable pair of signals by separating the real and imaginary parts of the microwave reflection coefficient of a SQUID by means of a 6-port network [25]. We found that these signals did not have a relationship usable to drive an up-down counter. We later confirmed this experimental finding with an electrical analog of the SQUID: the real and imaginary parts of the reflection coefficient have their peaks at the same rf power levels at the SQUID.

We then tried the arrangement shown in figure 23. It is a SQUID with a double readout circuit: one part generates the function $J_o(2\pi I/I_o)$, while the other generates the function $J_1(2\pi I/I_o)$. The circuit to display $J_o$ has already been described in chapter 4 of this report, and can be followed by referring to figure 20. The circuit to display the first order Bessel function $J_1$ is a heterodyne detector which uses the same L-band signal generator which drives the SQUID as a local oscillator. The signal reflected by the SQUID is mixed with a stronger signal at the driving frequency, and the product is amplified by a narrow-band IF amplifier, tuned to 30 MHz, before rectification. This picks out the sidebands of the reflected signal which are displaced from the driving frequency by 30 MHz. These sidebands are generated by the interaction between the microwave drive and the signal at 30 MHz to be detected by the SQUID. Their amplitude has the functional form $J_1(2\pi I/I_o)$. The meaning of negative values of this function is that the phases of the sidebands are reversed with respect to the incoming signal at 30 MHz. In order to preserve this phase information, the IF amplifier is biased with a signal of proper phase and amplitude derived from the same 30 MHz source. Finally, the component of the IF signal generated by the SQUID is separated out by a lock-in detector (the SQUID is modulated at a reference frequency of 1 kHz). The output of this lock-in detector has the functional form $J_1(2\pi I/I_o)$, where $I$ is the amplitude of the 30 MHz signal at the SQUID.

In order to drive a counter with the output of a lock-in detector, it is necessary to prevent false counts due to multiple crossing of the trigger threshold by noise. The technique is to introduce an electronic switch into the circuit. This will switch only when a signal over a certain threshold value follows a signal over the threshold with opposite sign. A suitable circuit, for which we thank Mr. Nolan V. Frederick,

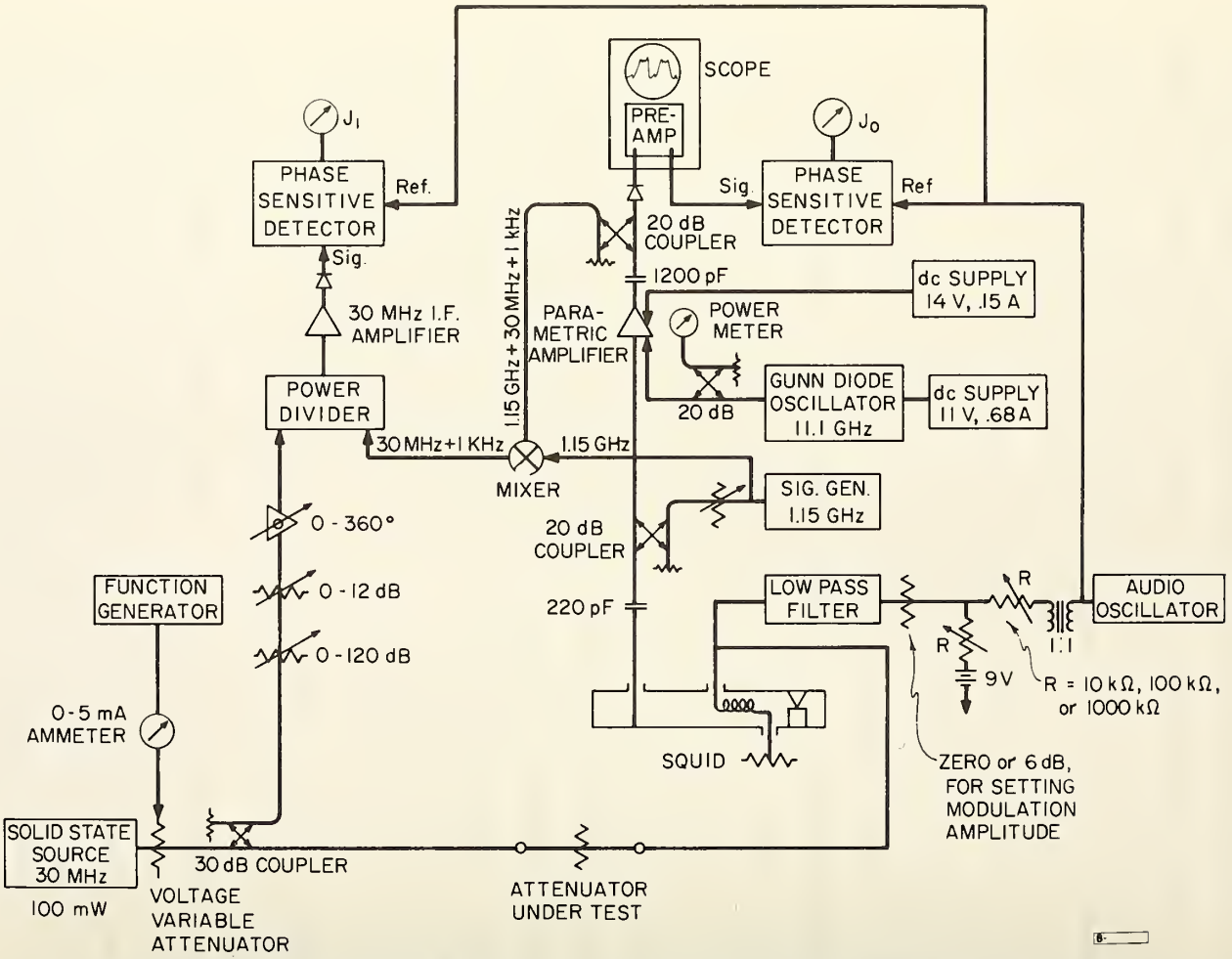


Figure 23. System for displaying the response functions $J_0(2\pi I/I_0)$ and $J_1(2\pi I/I_0)$ simultaneously, where I is the amplitude of the 30 MHz current at the input of the SQUID. This pair of signals would be suitable for driving an up-down counter.

is shown in figure 24. It is driven by the output of the lock-in detector, and in turn drives the counter.

We have assembled this system and had both readout channels working. Trials with an up-down counter remain for the future.

A simpler technique, which does not require an up-down counter, is to use a variable attenuator in the rf line to slowly shut off the 30 MHz signal at the SQUID. A simple counter can then be used to count the nulls of $J_o(2\pi I/I_o)$ as they are traversed in one direction only. We tried this technique using a function generator driving a voltage-variable attenuator at a suitably slow rate (figure 23). We were able to count 100 nulls without false counts after careful adjustment of the time constant of the lock-in detector and the (rather slow) counting rate. Optimum results would be obtained if the nulls were traversed at a steady rate. This requires proper shaping of the time-dependence of the output of the function generator to match the characteristics of the voltage-variable attenuator, to which we are giving further attention.

### 6.2 Interpolation Between Nulls

For many purposes it would be desirable to measure rf power or attenuation over a continuous range rather than just at points defined by the system. In particular, there are wide intervals (measured in dB) between the first few nulls of $J_o(2\pi I/I_o)$. Full interpolation between these points could be achieved with an auxiliary attenuator. Its dynamic range would not need to exceed 8 dB, but it would need to have small insertion loss, great accuracy, and a wide range of operating frequency. No such attenuator exists at present.

Alternatively, with proper calibration other properties of the function $J_o(2\pi I/I_o)$, in addition to the positions of the nulls, might be used for measurement.

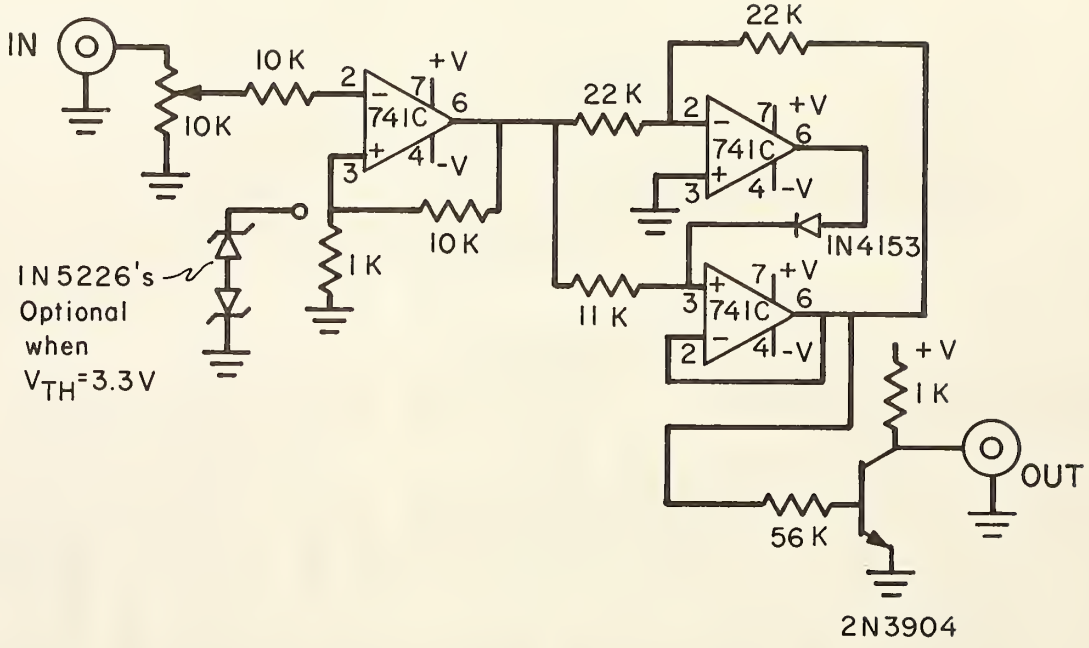


Figure 24. Trigger circuit for driving a counter from the output of a lock-in detector, designed by N. V. Frederick. This circuit introduces hysteresis to prevent spurious counts due to noise.

Another possibility is to use the combined display of $J_o(2\pi I/I_o)$ and $J_1(2\pi I/I_o)$ obtainable with the system shown in figure 23. Using both these functions together doubles the number of defined null points in a given range of power.

## 6.3 Increasing the Dynamic Range

The dynamic range obtainable by counting the nulls in the response of a single SQUID is limited in practice by the principle of diminishing returns: every 10 dB requires more than a three-fold increase in the number of nulls to count. It would probably be inconvenient to cover a range greater than 60 dB with a single SQUID. The simplest way to increase the dynamic range of an integrated system would be to use two or three SQUIDs, with sensitivities differing by 50 dB, in series on a common rf line. Insensitive SQUIDs are so weakly coupled to the rf input circuit that they constitute a negligible perturbation of the signal. The final, most sensitive SQUID could be matched to the characteristic impedance of the rf line to form the termination. Using L-band readout circuits, the additional cost of multiple units would be small.

## 6.4 Specialized Electronics

The systems for measuring power and attenuation which we described in chapters 3 and 4 of this report are strictly "breadboard" models. They were assembled using commercial signal generators, amplifiers, lock-in detectors, etc., which are much more versatile, and therefore expensive, than is required for their functions in the system. Now that the required operating conditions and signal levels are known, it is possible to design a much simpler, cheaper, system for the specialized purpose of interrogating the SQUIDs for the desired information.

## 6.5 Automatic Plotting

We already use a computer program to analyze the results of measurements with the SQUID systems (see chapter 4 of this report). It is not difficult to program the computer to plot, for example, a calibration curve for an attenuator directly with the information it stores and generates. The computer would then mathematically interpolate between the points at which actual measurements are made. To a certain extent this might serve as a substitute for making measurements over a continuous range.

## 7. SUMMARY

We have demonstrated a system for measuring rf power at levels down to $10^{-9}$ W with an uncertainty of about $\pm 0.1$ dB over a dynamic range of about 50 dB, in the range of frequency from 0 to 1 GHz. We have solved the foreseeable problems in extending the range of these measurements of power down to the order of $10^{-15}$ W.

We have demonstrated a system for measuring attenuation at 30 MHz over a dynamic range of about 50 dB. It agrees with the technique presently used by the NBS Calibration Service within random scatter of $\pm 0.002$ dB rms, which probably represents the uncertainty of setting the attenuator itself. Since this agreement is much closer than the limit of estimated systematic errors allowed on reports of calibration, it presents an opportunity to re-examine those errors and possibly revise the estimate.

This work is continuing, with the aim of making further refinements and extensions of these systems.

Acknowledgment. We would like to thank our colleagues, N. V. Frederick, J. E. Zimmerman, and D. B. Sullivan for their contributions to this work.

## REFERENCES


[1] J. E. Zimmerman and J. D. Siegwarth, Cryogenics 13, 158 (1973).

[2] B. D. Josephson, Rev. Mod. Phys. 36, 216 (1964).

[3] I. Giaever, Phys. Rev. Letters 5, 147 (1960).

[4] J. Clarke, Proc. Roy. Soc. (London) A308, 447 (1969).

[5] I. Giaever, Phys. Rev. Letters 20, 1286 (1968).

[6] P. W. Anderson and A. H. Dayem, Phys. Rev. Letters 13, 195 (1964).

[7] J. E. Zimmerman, 1972 Applied Superconductivity Conference (IEEE, New York, N.Y., 1972), p. 544.

[8] A. H. Silver and J. E. Zimmerman, Phys. Rev. 157, 317 (1967).

[9] J. E. Zimmerman, P. Thiene, and J. T. Harding, J. Appl. Phys. 41, 1572 (1970).

[10] D. B. Sullivan, Nat. Bur. Stand. (U.S.) Tech. Note 629, 40 pages (Nov. 1972).

[11] British Association Mathematical Tables, Vol. VI (1950).

[12] M. B. Simmonds and W. H. Parker, J. Appl. Phys. 42, 38 (1971).

[13] D. E. McCumber, J. Appl. Phys. 39, 3113 (1968).

[14] W. Schroen, J. Appl. Phys. 39, 2671 (1968).

[15] R. Graeffe and T. Wiik, J. Appl. Phys. 42, 2146 (1971).

[16] J. Seto and T. Van Duzer, Appl. Phys. Letters 19, 488 (1971).

[17] P. Cardinne, M. Marti et M. Renard, Revue de Physique Appliquee 6, 547 (1971).

[18] P. Cardinne, B. Manness, and M. Renard, 1972 Applied Superconductivity Conference (IEEE, New York, N.Y., 1972), p. 565.

[19] J. E. Zimmerman, J. Appl. Phys. 42, 30 (1971).

[20] J. J. Hauser, H. C. Theuerer, and N. R. Werthamer, Phys. Rev. 136, 637 (1964).

[21] Reference Data for Radio Engineers, ITT Corp., fourth edition (1956).

[22] R. A. Kamper, M. B. Simmonds, R. T. Adair, and C. A. Hoer, Proc. IEEE 61, 121 (1973).

[23] Nat. Bur. Stand. (U.S.) Spec. Publ. 250, (Dec. 1970).

[24] J. R. Waldram, Adv. Phys. 13, 1 (1964).

[25] C. A. Hoer, IEEE Trans. Instr. Meas. IM-21, 466 (1972).

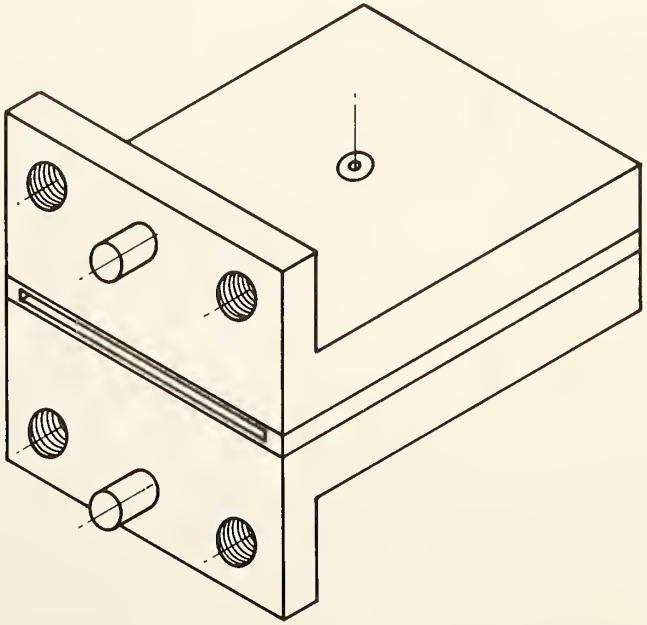

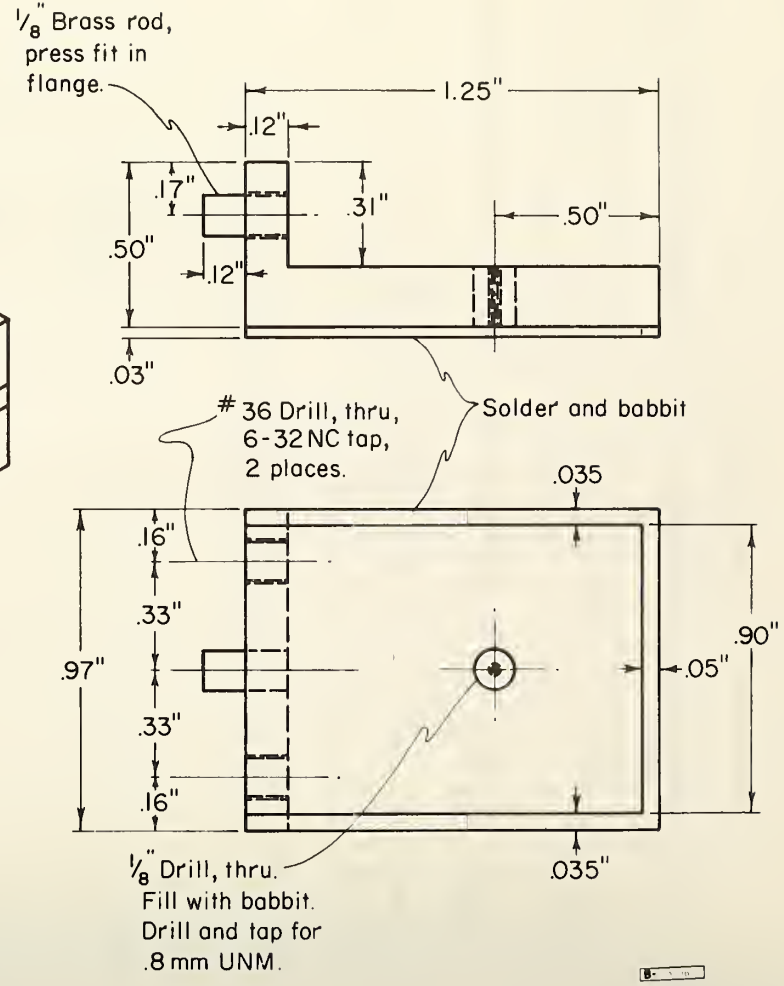


Figure 25. Details of construction of the X-band SQUID.

## APPENDIX: WORKSHOP NOTES

The X-band SQUID: Figure 25 shows the measurements of a typical X-band SQUID. Dimensional tolerances are about ± 10% except for the location of holes in the flange, which must be within ± 0.003 cm of their correct positions in order to avoid blocking the rather small waveguide.

We usually start by taking two pieces of 1 inch by 1/2 inch (2.5 cm x 1.3 cm) rectangular brass stock, 3.2 cm long, with ends milled square. We drill blind holes in the faces of these blocks in the places, around the point contact screws, where we will eventually want inserts of babbitt (see figures 2 and 3). We heat these blocks on a hotplate and tin the faces which will form the waveguide walls, using 50-50 lead-tin solder and an acid flux. After shaking off excess solder, we wash off the flux with water, reheat the blocks on the hotplate, and melt pools of babbitt onto the tinned faces. We do not use flux for this operation. We then cool the blocks and mill the babbitt-lined faces of the blocks to a thickness of 0.1 to 0.3 mm. This sometimes uncovers unacceptably large voids, requiring a second attempt at the tinning and casting. Once we obtain an acceptable babbitt surface we cut the blocks to the final shape shown in figure 25 with a milling machine. If the SQUID is to have a toroidal coupling coil, we cut the grove for it (1.5 mm x 1.5 mm) at this stage. To join the two halves of the SQUID, we clamp them together with a spacer, 0.25 mm thick and 2.3 cm wide, made of polyimide plastic. The blocks and the spacer are carefully lined up, with the square end of the spacer 2 mm inside the closed end of the SQUID. We then heat the whole assembly on the hotplate until 50-50 lead-tin solder will just melt. We then seal the sides and end of the SQUID with this solder. No flux is required: the solder appears to amalgamate with the surface of the babbitt. Care must be taken to avoid melting the babbitt. After cooling the SQUID and removing the spacer,

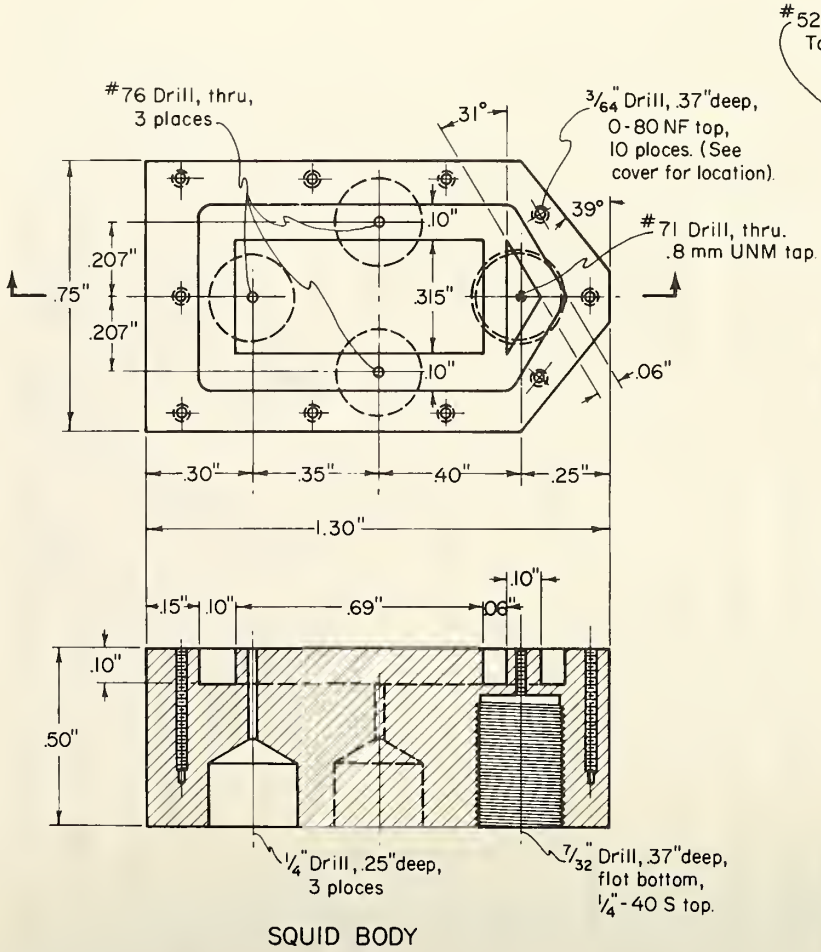


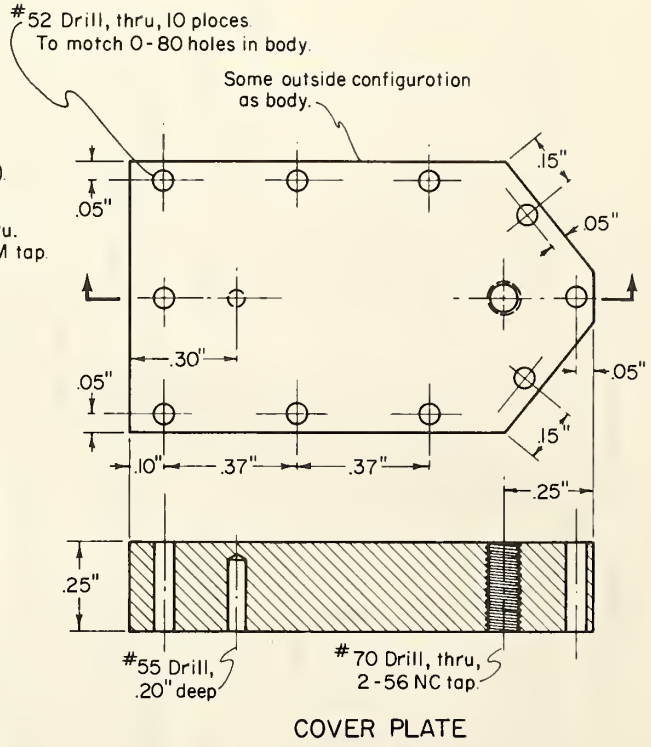


Figure 26. Details of construction of the L-band SQUID.

the outside of the SQUID is trimmed and the face of the flange is milled flat. When locating the holes for screws and locating pins in the flange, it is helpful to line it up with the mating flange using the same spacer that was used in connecting the two halves.

All connectors, etc., are attached to the completed SQUID either by screws or with a solder such as Rose metal or Wood's metal with a low melting point. We usually use SMA connectors.

The screws for the point contact are made from 1/32 inch (0.8 mm) niobium wire. The tips do not require accurate machining: we usually shape them by hand on a fine sharpening stone. The thread size we use is 0.8 mm UNM, with 50 threads per cm. Cutting threads in niobium requires care. It is best to use a chlorinated hydrocarbon for lubricant and to make very short cuts (1/4 turn) before breaking off and clearing the chips. There is no problem with babbitt: with any light lubricant it will take drills and taps easily. Levers of niobium can be attached to niobium screws by spot welding.

The L-band SQUID: The two halves of this object are made of solid babbitt, according to the dimensions shown in figure 26. Again, dimensional tolerances are ± 10%. The finished SQUID must resonate within the passband of the readout circuit at 1.2 GHz. This can be accomplished by trimming the metal parts or the dielectric spacer.

We had our SQUIDs machined by a computer-controlled milling machine. We would be happy to discuss the program with anyone having access to a similar facility.

Three SMA connectors are soldered to the body of the SQUID with Rose metal. Two of these are wired to the signal coil, while the third (which carries the L-band drive) is connected across the dielectric gap to the opposite side of the cavity. This is most conveniently done by

attaching a copper pin to the center conductor of the SMA connector, and pressing a matching socket into the lid of the SQUID. A suitable socket may easily be obtained by taking the center connector out of a female SMA connector.

The point contact is between a sharp-tipped 0.8 mm UNM screw, plated with a Pt-W alloy, and a plated niobium foil, 1 mm x 2 mm x 0.02 mm, as described in section 2.3 of this report. The niobium foil is spot welded to a 2-56 NC niobium screw. This passes through the lid of the SQUID and should be held in place by a lock nut. The small niobium screw passes through the main body of the SQUID. The far end is flattened to the shape of a screwdriver, which engages with a removable adjusting rod in a guide tube passing out through the top plate of the cryostat. A small leaf spring takes up the backlash of the screw when the drive is disconnected.

The SQUID is assembled by bolting the two halves together. The joint is then sealed (electrically) with Rose metal, applied with a soldering iron with no flux. The connectors are also soldered onto the body of the SQUID with Rose metal.

Cryostats and Plumbing: We will not describe the cryostats in detail: they were not specifically designed for this work and satisfactory commercial units are available. The cryostat should be about one meter long and wide enough to accommodate the SQUIDs. It is helpful to have a loose-fitting polystyrene foam plug in the upper 20 cm for a thermal radiation baffle. All metal connections passing into the liquid helium must be made of a material such as stainless steel with a low thermal conductivity. Since the electric currents they will carry are small, they should be as light as is compatible with mechanical requirements. We use stainless steel 50 $\Omega$ coaxial lines, with silver-plated inner conductors

and polyethylene dielectric. The X-band waveguide is also of stainless steel, with walls 0.25 mm thick. It is connected to the SQUID via a linear taper section 10 cm long, made of brass. The top of the cryostat, and all electrical connections there, are sealed leaving a single vent with a no-return valve to prevent condensation of air by the liquid helium. The cryostat is encased in a $\mu$-metal shield, 1 mm thick and 45 cm long, and an aluminum case, 3 mm thick, enclosing the whole cryostat. This latter is bolted to the brass top plate of the cryostat, so that the only electrical access to the interior is through the lines and waveguides passing through to the SQUIDs. These shields are designed to attenuate ambient electromagnetic noise.

FORM NBS-114A (1-71)

| U.S. DEPT. OF COMM. BIBLIOGRAPHIC DATA SHEET | 1. PUBLICATION OR REPORT NO. NBS TN-643 | 2. Gov't Accession No. | 3. Recipient's Accession No. |
|---|---|---|---|

**4. TITLE AND SUBTITLE**

Measurement of rf Power and Attenuation Using Superconducting Quantum Interference Devices

**5. Publication Date**

August 1973

**6. Performing Organization Code**

**7. AUTHOR(S)**

R. A. Kamper, M. B. Simmonds, C. A. Hoer, R. T. Adair

**8. Performing Organization**

**9. PERFORMING ORGANIZATION NAME AND ADDRESS**

NATIONAL BUREAU OF STANDARDS, Boulder Labs.
DEPARTMENT OF COMMERCE
Boulder, Colorado 80302

**10. Project/Task/Work Unit No.**

2750483

**11. Contract/Grant No.**

partially supported by CCG 72-72

**12. Sponsoring Organization Name and Address**

DoD Calibration Coordinating Group (CCG)
*Army Metrology Center, Huntsville, Alabama
Navy Metrology Center, Pomona, California
Air Force Metrology Center, Newark, Ohio
*1973 Chairman, M. L. Fruechtenicht, AMSMI-M

**13. Type of Report & Period Covered**

Annual Report for FY7

**14. Sponsoring Agency Code**

**15. SUPPLEMENTARY NOTES**

**16. ABSTRACT** (A 200-word or less factual summary of most significant information. If document includes a significant bibliography or literature survey, mention it here.)

This report is the product of the first two years' work on a project to exploit an entirely new principle for the measurement of rf power and attenuation, namely the Superconducting QUantum Interference Device (SQUID). This is a simple circuit of superconducting metal, operating at a very low temperature in a bath of liquid helium. It functions as a sensor of magnetic flux with an almost perfectly periodic response over a wide dynamic range. It may therefore be used to measure dc or rf electrical quantities such as current, power, attenuation, etc., in circuits inductively coupled to it. Measurements of these quantities can be made by counting off periods in the response of the SQUID (flux quanta) in the same way that we measure length with a laser by counting off wavelengths of light.

This work is partly funded by the CCG under project number 72-72. It has reached the stage of a demonstration that the new principle can indeed be used for precise measurement. We have developed and tested prototype systems for measuring power and attenuation as accurately as we can test by the conventional means available to us. A single calibration with dc is required to measure absolute rf power in the range of frequency from 0 to 1 GHz at levels from $10^{-8}$ W to $10^{-3}$ W with an uncertainty of ±0.1 dB at the port of the SQUID. Transferring this measurement to calibrate a source of power would require a proper evaluation of the intervening network over the full range of frequency. We have demonstrated the feasibility of extending our measurements of power to much lower levels. No external calibration is required to measure rf attenuation directly over a dynamic range of 45 dB with an rms deviation of ±0.002 dB from calibrations performed by the NBS Calibration Service.

After an elementary exposition of the basic principles of our technique, we describe: the SQUIDs themselves; the prototype systems we have developed to measure rf power and attenuation; systematic errors and fundamental limitations of the measurements that can be performed with them; and the obvious and immediate improvements that can be applied to them. We reserve an appendix for detailed drawings and instructions for the fabrication of components.

In order to make this report self-contained, we have included the material from previous reports that has successfully withstood the test of time.

**17. KEY WORDS** (Alphabetical order, separated by semicolons)

Josephson effect; quantum interference; rf attenuation; rf measurement; rf power; superconductivity.

**18. AVAILABILITY STATEMENT**

[x] UNLIMITED.

[ ] FOR OFFICIAL DISTRIBUTION. DO NOT RELEASE TO NTIS.

**19. SECURITY CLASS (THIS REPORT)**

UNCLASSIFIED

**21. NO. OF PAGES**

93

**20. SECURITY CLASS (THIS PAGE)**

UNCLASSIFIED

**22. Price**

$1.00

☆GPO 1973 — 784-568 REGION NO. 8

USCOMM-DC 66244-P71

# NBS TECHNICAL PUBLICATIONS

## PERIODICALS

**JOURNAL OF RESEARCH** reports National Bureau of Standards research and development in physics, mathematics, and chemistry. Comprehensive scientific papers give complete details of the work, including laboratory data, experimental procedures, and theoretical and mathematical analyses. Illustrated with photographs, drawings, and charts. Includes listings of other NBS papers as issued.

*Published in two sections, available separately:*

- **Physics and Chemistry (Section A)**

Papers of interest primarily to scientists working in these fields. This section covers a broad range of physical and chemical research, with major emphasis on standards of physical measurement, fundamental constants, and properties of matter. Issued six times a year. Annual subscription: Domestic, $17.00; Foreign, $21.25.

- **Mathematical Sciences (Section B)**

Studies and compilations designed mainly for the mathematician and theoretical physicist. Topics in mathematical statistics, theory of experiment design, numerical analysis, theoretical physics and chemistry, logical design and programming of computers and computer systems. Short numerical tables. Issued quarterly. Annual subscription: Domestic, $9.00; Foreign, $11.25.

### TECHNICAL NEWS BULLETIN

The best single source of information concerning the Bureau's measurement, research, developmental, cooperative, and publication activities, this monthly publication is designed for the industry-oriented individual whose daily work involves intimate contact with science and technology—*for engineers, chemists, physicists, research managers, product-development managers, and company executives.* Includes listing of all NBS papers as issued. Annual subscription: Domestic, $6.50; Foreign, $8.25.

## NONPERIODICALS

**Applied Mathematics Series.** Mathematical tables, manuals, and studies.

**Building Science Series.** Research results, test methods, and performance criteria of building materials, components, systems, and structures.

**Handbooks.** Recommended codes of engineering and industrial practice (including safety codes) developed in cooperation with interested industries, professional organizations, and regulatory bodies.

**Special Publications.** Proceedings of NBS conferences, bibliographies, annual reports, wall charts, pamphlets, etc.

**Monographs.** Major contributions to the technical literature on various subjects related to the Bureau's scientific and technical activities.

**National Standard Reference Data Series.** NSRDS provides quantitative data on the physical and chemical properties of materials, compiled from the world's literature and critically evaluated.

**Product Standards.** Provide requirements for sizes, types, quality, and methods for testing various industrial products. These standards are developed cooperatively with interested Government and industry groups and provide the basis for common understanding of product characteristics for both buyers and sellers. Their use is voluntary.

**Technical Notes.** This series consists of communications and reports (covering both other-agency and NBS-sponsored work) of limited or transitory interest.

**Federal Information Processing Standards Publications.** This series is the official publication within the Federal Government for information on standards adopted and promulgated under the Public Law 89–306, and Bureau of the Budget Circular A–86 entitled, Standardization of Data Elements and Codes in Data Systems.

**Consumer Information Series.** Practical information, based on NBS research and experience, covering areas of interest to the consumer. Easily understandable language and illustrations provide useful background knowledge for shopping in today's technological marketplace.

## BIBLIOGRAPHIC SUBSCRIPTION SERVICES

**The following current-awareness and literature-survey bibliographies are issued periodically by the Bureau:**

**Cryogenic Data Center Current Awareness Service** (Publications and Reports of Interest in Cryogenics). A literature survey issued weekly. Annual subscription: Domestic, $20.00; foreign, $25.00.

**Liquefied Natural Gas.** A literature survey issued quarterly. Annual subscription: $20.00.

**Superconducting Devices and Materials.** A literature survey issued quarterly. Annual subscription: $20.00. Send subscription orders and remittances for the preceding bibliographic services to the U.S. Department of Commerce, National Technical Information Service, Springfield, Va. 22151.

**Electromagnetic Metrology Current Awareness Service** (Abstracts of Selected Articles on Measurement Techniques and Standards of Electromagnetic Quantities from D-C to Millimeter-Wave Frequencies). Issued monthly. Annual subscription: $100.00 (Special rates for multi-subscriptions). Send subscription order and remittance to the Electromagnetic Metrology Information Center, Electromagnetics Division, National Bureau of Standards, Boulder, Colo. 80302.

Order NBS publications (except Bibliographic Subscription Services) from: Superintendent of Documents, Government Printing Office, Washington, D.C. 20402.

**U.S. DEPARTMENT OF COMMERCE**
**National Bureau of Standards**
Washington, D.C. 20234

OFFICIAL BUSINESS

Penalty for Private Use, $300

POSTAGE AND FEES PAID
U.S. DEPARTMENT OF COMMERCE
COM-215